

MANOOP CHENCHILIYAN

Nano-structural Constraints for the
Picosecond Excitation Energy Migration
and Trapping in Photosynthetic
Membranes of Bacteria



MANOOP CHENCHILIYAN

Nano-structural Constraints for the
Picosecond Excitation Energy Migration
and Trapping in Photosynthetic
Membranes of Bacteria



This study was carried out at the Institute of Physics, University of Tartu.

The Dissertation was admitted on December 13, 2016, in partial fulfillment of the requirements for the degree of Doctor of Philosophy in physics, and allowed for defense by the Council of the Institute of Physics, University of Tartu.

Supervisor: Prof. Arvi Freiberg, DSc. Institute of Physics and Institute of Molecular and Cell Biology, University of Tartu, Estonia.

Opponent: Dr. Esa Tyystjärvi, Molecular Plant Biology, Department of Biochemistry, University of Turku, Turku, Finland.

Defense: January 27, 2017, at 15.00, Auditorium B103, Physicum, W. Ostwald Str. 1, University of Tartu, Tartu, Estonia.

This work has been supported by European Social Fund's Doctoral Studies and Internationalization Programme DoRa, which is carried out by Archimedes Foundation. Partial financial support provided by the Estonian Research Council grant IUT02-28.



ISSN 1406-0647

ISBN 978-9949-77-325-1 (print)

ISBN 978-9949-77-326-8 (pdf)

Copyright: Manoop Cenchiliyan, 2016

University of Tartu Press

www.tyk.ee

TABLE OF CONTENTS

LIST OF ORIGINAL PUBLICATIONS	7
1. INTRODUCTION.....	9
1.1. General perspective of photosynthesis	9
1.2. Overview of the photosynthetic machinery of non-sulphur purple bacteria	10
1.2.1. Basic components of a chromatophore vesicle involved in light reactions	13
1.2.1.1. The peripheral light harvesting complex 2.....	13
1.2.1.2. The core RC-LH1 complexes.....	15
1.2.1.3. The reaction centre	17
1.2.2. Adaptation of intracytoplasmic membranes into different levels of light intensities.....	18
1.3. Exciton interpretation of the bacterial spectra	20
1.4. Excitation energy transfer and trapping process in the photosynthetic unit	23
1.4.1. Excitation energy transfer – A brief theoretical overview ...	23
1.4.2. Factors that influence the energy trapping time in the core complex	26
1.4.3. Kinetic model of exciton population dynamics in the photosynthetic unit of purple bacteria	27
1.4.4. Quantum efficiency of energy trapping.....	30
1.5. Steady state and picosecond time resolved fluorescence spectroscopy as the method to study primary processes of photosynthesis	31
2. RESEARCH OBJECTIVES	33
3. EXPERIMENTAL	34
3.1. Samples.....	34
3.2. Sample Preparation for Optical Studies.....	36
3.3. Spectroscopy.....	37
3.3.1. Steady-State Fluorescence Spectroscopy	37
3.3.2. Picosecond Time-resolved Fluorescence Spectroscopy	38
3.4. Data Analysis.....	41
4. RESULTS	43
4.1. Efficiency of Light Harvesting in <i>Rhodobacter sphaeroides</i> Adapted to Different Levels of Light (Paper I)	43
4.2. Dimerization of Core Complexes as an Efficient Strategy for Energy Trapping (Paper II).....	45
4.3. Spectral and Kinetic Effects Accompanying the Assembly of Core Complexes (Paper III).....	48
5. SUMMARY AND FURTHER CHALLENGES.....	52

SUMMARY IN ESTONIAN	54
ACKNOWLEDGEMENTS	56
REFERENCES.....	58
PUBLICATIONS	69
CURRICULUM VITAE	107
ELULOOKIRJELDUS.....	109

LIST OF ORIGINAL PUBLICATIONS

The current thesis is based on the following original publications, referred to in the text by their associated Roman numerals (the author's contribution is indicated in parenthesis).

- I. Timpmann, Kõu; **Chenchiliyan, Manoop**; Jalviste, Erko; Timney, John A; Hunter, C. Neil; Freiberg, Arvi (2014). Efficiency of light harvesting in a photosynthetic bacterium adapted to different levels of light. *Biochimica et Biophysica Acta-Bioenergetics*, 1837(10), 1835–1846. (Performed most of the experiments, participated in analyses of the data and in writing the manuscript.)
- II. **Chenchiliyan, Manoop**; Timpmann, Kõu; Jalviste, Erko; Adam, G. Peter; Hunter, C. Neil; Freiberg, Arvi (2016). Dimerization of core complexes as an efficient strategy for energy trapping in *Rhodobacter sphaeroides*. *Biochimica et Biophysica Acta-Bioenergetics*, 1857 (6), 634–642. (Participated in designing the study, performed the experiments, analysed the data and wrote much of the manuscript.)
- III. Freiberg, Arvi; **Chenchiliyan, Manoop**; Rätsep, Margus; Timpmann, Kõu (2016). Spectral and kinetic effects accompanying the assembly of core complexes of *Rhodobacter sphaeroides*. *Biochimica et Biophysica Acta-Bioenergetics*, 1857 (11), 1727–1733. (Performed the fluorescence lifetime measurements, fitted the kinetic data and prepared the figures for the publication.)

The results of the thesis work have been reported in the following international and national scientific forums (the presenter is shown in bold).

- March 2013 **Manoop Chenchiliyan**, Kõu Timpmann, Arvi Freiberg. Poster presentation at University of Tartu and Tallinn Technical University doctoral school, Functional materials and technologies, Tallinn, Estonia. “Excitation light intensity dependence of energy transfer and trapping efficiencies in photosynthetic purple bacteria”.
- Dec. 2013 **Manoop Chenchiliyan**, Kõu Timpmann, Erko Jalviste, C. Neil Hunter, Arvi Freiberg. Oral presentation at “Annual conference”, Institute of molecular cell biology, University of Tartu, Estonian bio centre and Genome centre Tartu, Estonia. “Excitation intensity-dependent picosecond fluorescence from photosynthetic bacteria adapted to different levels of light”.
- June 2014 **Arvi Freiberg**, Kõu Timpmann, Manoop Chenchiliyan, Erko Jalviste, John A. Timney, C. Neil Hunter. Invited talk at “Photosynthesis Research for Sustainability-2014”, Puschino, Russia. “Light harvesting in photosynthetic bacteria acclimated to different levels of light”.
- Oct. 2014 Kõu Timpmann, **Manoop Chenchiliyan**, Erko Jalviste, John A. Timney, C. Neil Hunter, Arvi Freiberg. Poster presentation at

- “12th Nordic Photosynthesis Congress”, University of Uppsala, Sweden. “Efficiency of light harvesting in a photosynthetic bacterium adapted to different levels of light”.
- Oct. 2014 **Arvi Freiberg**, Manoop Chenchiliyan, Kõu Timpmann. Invited talk at COST PHOTOTECH Training School on "Advanced Laser Spectroscopy in Green Phototechnology", Szeged, Hungary. ““Biological Variability” in the Research of Photosynthetic Light Harvesting”.
- Dec. 2014 **Manoop Chenchiliyan**, Kõu Timpmann, C. Neil Hunter, Peter G. Adams, Arvi Freiberg. Oral presentation at Annual conference, Institute of molecular cell biology, University of Tartu, Estonian bio centre and Genome centre Tartu, Estonia. “Excitation energy trapping in *Rhodobacter sphaeroides* with monomeric and dimeric core complexes”.
- Sep. 2015 Kõu Timpmann, Manoop Chenchiliyan, Liina Kangur, **Arvi Freiberg**. Oral presentation at The International Conference on Charge Transfer and Transport at the Nanoscale (CTTN15), Santiago de Compostela, Spain. “High-pressure Tuning of Pico-second-range Electron Transport in Photosynthetic Reaction Center Proteins”.
- Jan. 2016 **Manoop Chenchiliyan**, Kõu Timpmann, Erko Jalviste, Peter G. Adams, C. Neil Hunter, Arvi Freiberg. Poster presentation at XX International School of Pure and Applied Biophysics, Instituto Veneto di Scienze Lettere ed Arti, Venice, Italy. “Dimerization of core complexes as an efficient strategy for energy trapping in *Rhodobacter sphaeroides*”.
- Feb. 2016 Manoop Chenchiliyan, Liina Kangur, Kõu Timpmann, **Arvi Freiberg**. Invited talk at 8th International Meeting on Biomolecules under Pressure (IMBP), Dortmund, Germany. “Pressure Tuning of Primary Photochemistry”.
- June 2016 Manoop Chenchiliyan, Kõu Timpmann, **Arvi Freiberg**. Invited talk at “Photosynthesis Research for Sustainability-2016”, Puschino, Russia. “Structural Constraints for Excitation Energy Migration and Trapping in Photosynthetic Bacteria”.
- June 2016 Manoop Chenchiliyan, Kõu Timpmann, Erko Jalviste, **Arvi Freiberg**. Oral presentation at 12th International Conference on Diffusion in Solids and Liquids (DSL 2016) Split, Croatia. “Nano-structural Constraints for Ultrafast Excitation Energy Diffusion and Transport in Photosynthetic Membranes”.

1. INTRODUCTION

1.1. General perspective of photosynthesis

Photosynthesis is a remarkable biological process that converts the solar energy into chemical energy either by plants, algae, or photosynthetic bacteria [1-5]. Although exploring so far into the past is difficult and uncertain in interpreting, the geochemical data suggest that the earliest versions of photosynthesis emerged about 3.8–3.4 billion years ago [6]. This was a dawn to life that begun to rely primarily on the abundant, ubiquitous and reliable energy source—the sunlight. Since then the photosynthesis had an incredible impact on the evolution of our planet and the life on it [7].

The annual rate of energy captured by photosynthesis is approximately 100 TW, while the energy consumption rate by the entire human civilization is 16 TW per year, which is almost six times smaller than the energy gained through photosynthesis [8]. At present about 85 % of the total global energy needs are fulfilled by fossil fuels. Eventually the readily available reserves of fossil fuels become scarce. However, rather than pending deficiency of fossil fuel, the major problem that the world is facing is the consequences of combustion of fossil fuels—an increasing release of CO₂ and other greenhouse gases into the atmosphere that has a direct impact on global climate change and well-being of the mankind [9-11]. To this end, there is dire need for alternative energy sources that can simultaneously meet the world's energy demands and reduce CO₂ emission. In fact we have existing technologies that can directly capture sunlight and produce electricity [12-15]. However these photovoltaic systems still need significant improvement towards increasing their efficiency as well as to reduce their cost in order to effectively compete with and finally replace fossil fuels. Alternatively, one can either utilize the molecular machineries of photosynthesis as an active photovoltaic material in the form of bio-hybrid devices [16, 17] or, employing the concepts of natural photosynthesis with cheap synthetic material into completely operational solar-to-fuel devices, in the form of artificial photosynthesis [18, 19]. Before collecting the enormous untapped potential of solar energy towards the global energy needs through the concepts of photosynthesis, one needs to learn thoroughly how it works in nature. This is a general objective of this thesis.

The earliest version of photosynthesis was almost certainly anoxygenic, i.e. it used inorganic compounds such as sulphide/elemental sulphur or molecular hydrogen in the bacterial environment as the electron donor for carbon dioxide reduction. However by about 2.3 billion years ago, oxygen began to accumulate in significant amounts on Earth atmosphere through oxygenic photosynthesis, which splits water in order to reduce carbon dioxide [6, 20]. Photosynthesis carried out by higher plants, algae and cyanobacteria are oxygenic, whereas in photosynthetic non-sulphur purple bacteria, the main interest of the current thesis, it is anoxygenic. In either form of photosynthesis, the primary processes involve absorption of photons by light-harvesting complexes (LHs), a rapid and

efficient excitation energy transfer from LHs to the reaction centre (RC) and the primary photochemical charge separation followed by the transmembrane electron transport [21, 22]. These processes are generally specified as ‘light reactions’. Leaving details aside, further steps known as the ‘dark reactions’ towards the production of the major cellular fuel, adenosine triphosphate (ATP) are performed, mediated by the cytochrome bc_1 , cytochrome c_2 and ATP synthase protein complexes. The electron returns to P870 at the end of the chain so it can be used again once light excites the reaction-center. Compared with bacteria, studying the complicated processes of photosynthesis is notably more challenging in oxygenic photosynthetic organisms due to their evolutionarily more advanced supramolecular structure [23, 24]. Hence, motivated by the availability of high-resolution structures of the major LH and RC proteins, and a detailed knowledge of the biogenesis and organisation of the bacterial photosynthetic membranes, this thesis inspects the primary processes of photosynthesis exclusively in a photosynthetic purple bacterium, *Rhodobacter (Rba.) sphaeroides*.

The relevant length scale in photosynthetic light harvesting ranges from the size of wavefunction of a localized electron, $\sim 1\text{\AA}$, to the size of a fully functional chromatophore that incorporate all the necessary pigment-protein complexes, $\sim 10^3\text{\AA}$. Likewise, the relevant timescales for an efficient excitation energy transfer ranges from $<100\text{ fs}$ (within the B850 and B875 ring respectively of LH2 and LH1, see following sections) to 1–2 ns, the singlet excited-state lifetime of LH1 ring [25]. In this work we study the influence of the nanostructural arrangement of either the chromatophore or solely the constituent transmembrane protein complexes from *Rba. sphaeroides* on the ultrafast excitation energy transfer and trapping.

1.2. Overview of the photosynthetic machinery of non-sulphur purple bacteria

In purple phototrophic bacteria, such as *Rba. sphaeroides*, the photosynthetic apparatus is found in invaginations of the cytoplasmic membrane termed the intracytoplasmic membrane (ICM). It is known from the earlier studies [26] that the ICM comprised of vesicles-like structures of 40–60 nm in *Rba. sphaeroides*. This aspect of ICM, in fact deny the historically proposed connectivity between the ICM [27–29] as well as the recently reported [30] continuous three dimensional vesiculated reticulum of ICM. Here we follow the more popular discrete vesicular outlook of the ICM in *Rba. sphaeroides* as shown in Fig. 1.1A and recently reviewed in [31]. Furthermore, it is important to notice that no aspect of this thesis is directly associated with the precise topology of the ICM. The duly purified from the cells ICM vesicles are named as ‘chromatophores’. Being equipped with all of the proteins (detailed further below) required for photosynthesis they can function independently [32]. A typical chromatophore vesicle contains thousands of pigment molecules (mostly bacteriochlorophyll-a

(BChl) and various carotenoids) distributed over hundreds of proteins to form a well-organized network of pigment-protein complexes [33-36]. The first steps of bacterial photosynthesis involve two basic types of pigment-protein complexes, (i) the ‘core complex’ comprised of a light harvesting complex 1 (LH1) and one or two RCs, and (ii) a ‘peripheral or distal’ light harvesting complex 2 (LH2). The photosynthetic RCs and the related LHs collectively form a functional unit called the photosynthetic unit (PSU) [37-39]. Some photosynthetic purple bacteria such as *Rhodospirillum rubrum* develop only core complexes. However, those bacteria that possess distal antennae apart from the core, the number of peripheral complexes varies with the growth light intensity [40].

The supramolecular atomic structural model of a typical chromatophore vesicle from *Rba. sphaeroides* with a diameter of 50 nm grown under low light intensities is depicted in Fig 1.1 (top) adopted from [34]. This model shows the major components of bacterial photosynthesis as discussed above and will be further detailed below.

The absorption spectrum of the low-light adapted (see section 1.2.2) chromatophore from *Rba. sphaeroides* in a buffer solution is presented in the panel B of Fig 1.1. The absorption bands can be assigned to associations of different pigment molecules within the chromatophore. A major portion of this spectrum is due to BChl molecules; however the absorption through the spectral window 400 nm to 500 nm is mainly facilitated by carotenoids. The absorption spectrum of the carotenoid is structured due to strong intra-molecular electron-vibrational coupling. Besides the light harvesting function in the spectral window that is inaccessible to BChls [41] and the role in structural stability (see section 1.2.1.1), the major function of carotenoid is to protect the bacterial photosynthesis from the potentially harmful photo-destructive reaction which occurs in the presence of oxygen [42]. The chemical structure of BChl, the dominant pigment molecule in a chromatophore, is illustrated in the inset of panel B of Fig 1.1. Its core is composed of four connected pyrrole rings (indicated I through IV) and a central magnesium atom. The molecular orbitals of BChl are delocalised over a large distance in the molecular plane (~1 nm) that determines their unique photo-physical and spectroscopic properties utilized by photosynthesis.

The main chromatophore bands of BChl origin in the near-IR spectral range peak around 800 nm, 850 nm and 875 nm, as shown by arrows. They are due to the transition into the lowest singlet excited state Q_y . The former two peaks, often called B800 and B850 are related to the peripheral LH2 complex, while the third, B875, to the LH1 complex, see Fig. 1.5 below for detailed decomposition of the spectrum. The weaker absorption band peaking around 590 nm, named the Q_x band, is a composite band which results from the transition into the second lowest excited singlet state of all the BChl molecules involved. The transition into the two overlapping higher energy singlet states termed B_x and B_y (commonly called a Soret band) gives rise to an absorption band in the near-UV region below ~400 nm. Together the BChl and carotenoid pigments of purple bacteria absorb the sunlight in a spectral region that is complementary to the oxygenic phototrophs, see the grey shaded area in Fig 1.1B.

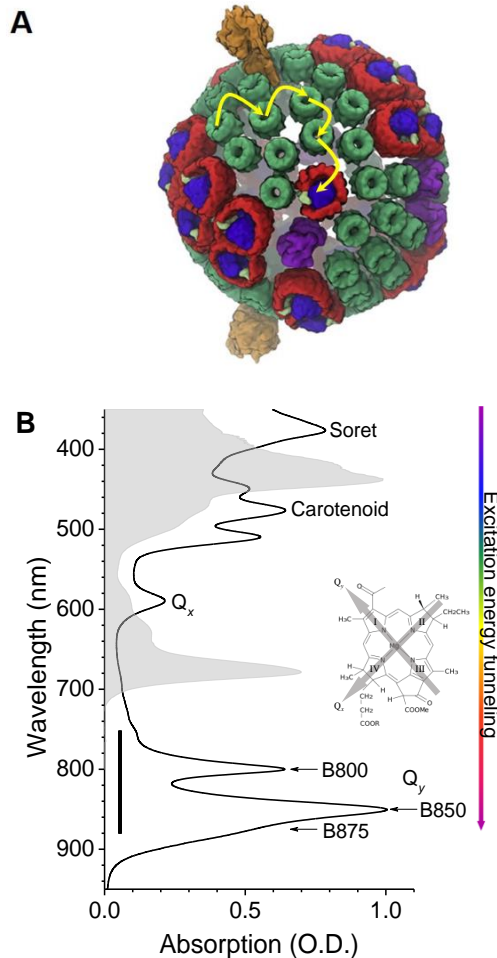


Fig. 1.1. (A) Atomic structural model of a chromatophore vesicle depicting constituent light-harvesting proteins. This vesicle features the low-light adapted model for *Rba. sphaeroides*, containing an enhanced number of peripheral antenna complexes LH2. The major integral membrane proteins are indicated by the following colours: LH2: dark green; LH1: red; PufX: light green; RC: blue; *cytbc*₁ dimers: purple; ATP synthases orange. Yellow arrows illustrate the directional excitation energy transfer along the membrane surface between different pigment-protein complexes. (B) The electronic (or rather electron-vibrational) absorption spectrum of a chromatophore vesicle in the near-UV, visible and near-IR spectral range with the traditional assignment of different bands. The approximate Q_y exciton band spread of the LH1 and LH2 complexes is designated by a thick black line. Decomposition of the spectrum in the Q_y range into its LH2 and RC-LH1 components is shown in Fig. 1.5. The inset of panel B shows the chemical structure of a BChl pigment. The direction of the Q_y and Q_x transition dipoles within the BChl molecule are shown by the grey arrows. The multi-coloured vertical arrow qualitatively indicates the “down-hill” funnelling of energy to the RC. The grey shaded area illustrates the reference absorption spectrum of a Photosystem I from the green plant *Arabidopsis thaliana*. See text for further details.

From the point of view of the photosynthesis primary processes, which involve excitation energy transfer and trapping, the most relevant electronic states are the lowest-energy Q_y excited electronic states of BChl. While for monomeric BChl molecules the Q_y transition appears as a single absorption band around 770 nm – 780 nm in different solvents, the BChl pigments in chromatophore gives rise to three separate spectral maxima belonging to two different pigment-protein complexes as highlighted above. The nature has taken smart care in arranging spatial and spectral coordinates of the involved chromoproteins such that the LH2 complexes, which absorb higher-energy light (corresponding absorption maxima at 800 and 850 nm) are placed in periphery with respect to the RC trap and the LH1 complexes absorbing lower-energy light (875 nm), closely surround the RCs. Driven by the thermodynamic free energy difference, this correlated spatial and spectral ordering warrants excitation energy relaxation to the lowest-energy electronic states within each and every pigment-protein complex as well as an almost unidirectional excitation energy transfer between different pigment-protein complexes along the photosynthetic membrane towards the RC with minimal losses. These processes are highlighted in Fig. 1.1 by coloured arrows.

The major modifications in the Q_y transition properties taking place upon assembly of the pigments in a protein environment occur by the interactions with the neighbouring pigments (causing exciton effects) and with the protein surroundings (inducing solvation effects such as solvent shift). Instrumental for exciton effects is precise relative positioning and orientation of the pigments in the protein scaffold. These issues will be further detailed in the following sections.

1.2.1. Basic components of a chromatophore vesicle involved in light reactions

This section briefly details the structural features of the individual pigment-protein complexes of a chromatophore vesicle that are involved in the light reactions studied.

1.2.1.1. The peripheral light harvesting complex 2

The structure of the LH2 complex in different species of purple phototrophic bacteria has been obtained by X-ray crystallography [43, 44]. Among these, the structure of *Rhodospseudomonas (Rps.) acidophila* has been determined at a highest resolution of 2.0 Å [45], showing atomic details of the pigment and protein molecules. Although the structure of LH2 from *Rba. sphaeroides* is determined only to 8 Å precision [46], it is widely speculated that it is similar to the structure of LH2 from *Rps. acidophila*, the view we generally adopt in this work.

The crystal structure of LH2 from *Rps. acidophila* is shown in Fig. 1.2, left hand side of panel A. It forms a nonameric ring of dimeric α -helical protein subunits. These basic transmembrane building blocks bind one carotenoid and three BChls pigment molecules. When linked together, the 27 BChl molecules scaffolding between an inner (α -helix) and outer (β -helix) walls of a hollow membrane-spanning protein cylinder form two separate rings of BChls, as shown in right hand side of Fig. 1.2. The BChls are non-covalently ligated to amino acid residues of the transmembrane helices via their central Mg atom and the hydrogen-bonded carbonyl side-groups. The membrane-spanning carotenoids contact BChls closely via intertwined phytol tails of the latter, important for the stability of the complex [47, 48].

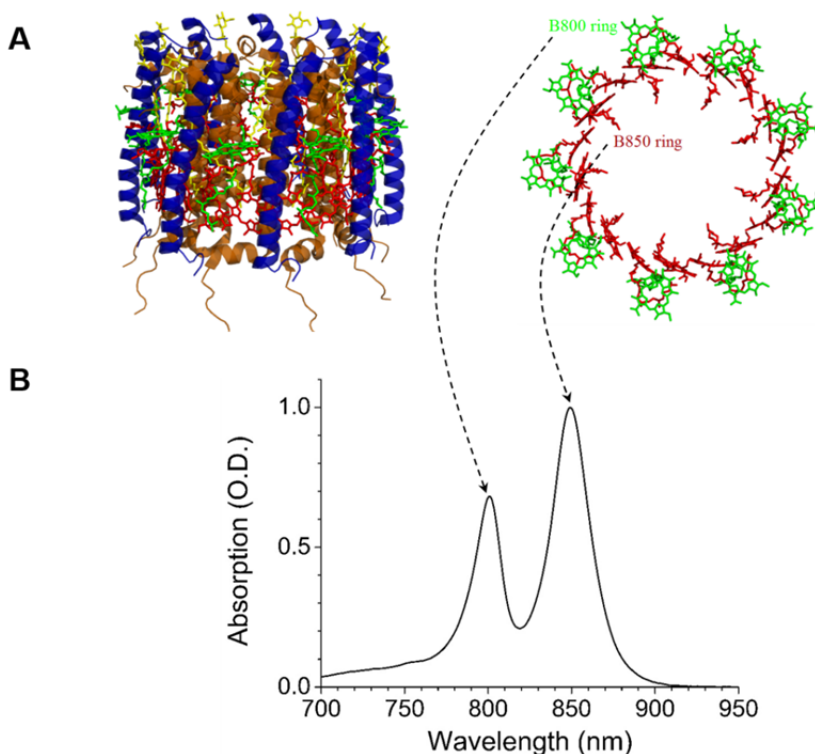


Fig. 1.2. (A) Left hand side: Structure of LH2 complex from *Rps. acidophila* as viewed from the side, showing the placement of the pigment molecules. Each subunit comprised of two transmembrane helices, called the α -helix (orange) and the β -helix (blue), three BChls (green/red) and one carotenoid molecule (yellow). The diameter of this cylindrical structure is about 65 Å. Right hand side: The structure of the BChl pigment rings responsible for the two intense absorption bands in the near-IR spectral range of LH2. The dashed arrows indicate the assignment of the rings with their corresponding absorption bands. The structures were produced using the pdb data by PyMOL. (B) Absorption spectrum of the LH2 complex from *Rba. sphaeroides*. See text for further details.

As mentioned in section 1.2, in contrary to monomeric BChl molecules, the Q_y transition in the LH2 complex gives rise to two absorption bands instead of one in the former case, although the BChl are chemically identical. This is due to the highly ordered arrangement of the BChl molecules into two concentric rings within the protein walls, named B800 and B850 according to their main absorption band maximum position. Such an arrangement of BChl pigments within the LH2 ring is illustrated on the right hand side of panel A in Fig. 1.2, where the proteins and carotenoid pigments were omitted for clarity. Among the 27 BChl pigments in LH2, the 18 red coloured pigments form a closely interacting ring towards the periplasmic (inside) side of the membrane, with their individual BChl molecular planes oriented perpendicular to the membrane plane. In this ring the adjacent BChls are separated by Mg-to-Mg distance of less than 10 Å. As a result of the close arrangement of the pigments in the B850 ring, large value of the Q_y transition dipole moments, and their proper orientation, they can strongly interact with each other via transition dipole-transition dipole (exciton) coupling mechanism [49, 50]. Dominating excitonic effects evident in the B850 spectrum include large spectral red shift, asymmetric shape relative narrowness, and extra strong (compared to monomeric BChl) dipole strength of the 850-nm absorption band [51]. The remaining 9 BChls coloured green form a ring with their individual molecular planes oriented roughly parallel to the membrane plane. These molecules responsible for the B800 band are widely separated holding a centre-to-centre distance of 21 Å; they are thus relatively weakly coupled. The observed spectral tuning of the B800 band relative to the absorption of isolated pigments is mainly caused by the hydrogen bonding of the B800 pigments with the surrounding protein [52].

1.2.1.2. The core RC-LH1 complexes

The LH1 complex encircles the RC and forms a supra-molecular complex, RC-LH1, named the core complex. Although the architecture of LH2 is relatively consistent, the core complex design varies from species to species with different configurations of the LH1 $\alpha\beta$ -heterodimers surrounding the RC. The LH1 forms a closed ring or closed ellipse around the RC, for example, in *Rhodospirillum rubrum*, *Rhodopseudomonas viridis*, *Rhodospirillum photometricum*, and in *Thermochromatium (T.) tepidum* [53-56], whereas some species of photosynthetic bacteria like *Rba. sphaeroides* and *Rhodopseudomonas (Rps.) palustris* hold an additional polypeptide, PufX in *Rba. sphaeroides* and W in case of *Rps. palustris*, which creates a gap in the LH1 ring around the RC [57-59]. It has been suggested that this gap enables quinones/quinols to cross the LH1 barrier [38, 60] and diffuse to the cytochrome bc1 complex, a key requirement for the cyclic electron transport and for the efficient photosynthetic growth [61]. As reviewed in Ref. [62], the presence of PufX polypeptide in wild type (WT) *Rba. sphaeroides* leads most of the core complexes to assemble into S-shaped dimeric structures [63-

66], while a small percentage remains as closed-ring-shaped PufX-containing monomers [34].

Recently a high quality X-ray structure of the RC-LH1 core complex was determined at 3.0 Å from *T. tepidum* [53]. This structure showed that the RC is completely surrounded by the LH1 ring of 16 $\alpha\beta$ -subunits. The LH1 forms an elliptical double-ring. The lengths of its major and minor axes are 82Å and 73Å for the inner ring and 105Å and 96Å for the outer ring, respectively. No such high resolution structure exists for the RC-LH1 core complex for *Rba. sphaeroides*, but numerous low resolution structures exist and models have been built [63-65, 67-69]. Figure 1.3 A shows the structure of the RC-LH1-PufX dimer with a small gap in the LH1 structure at the RC Q_B site, provided by the positioning of PufX [63-65]. Each RC is surrounded by the LH1 antenna, which comprises an inner ring of 14 LH1 α polypeptides, an outer ring of 14 LH1 β polypeptides, and two BChls sandwiched between each $\alpha\beta$ pair of trans-membrane helices. The two halves of the dimer have a nearly two-fold symmetry and are inclined towards each other (see Fig 1.3 A left hand side) at an angle of $\sim 146^\circ$ [63]. This significant bend in the complex was proposed to be important in inducing membrane curvature.

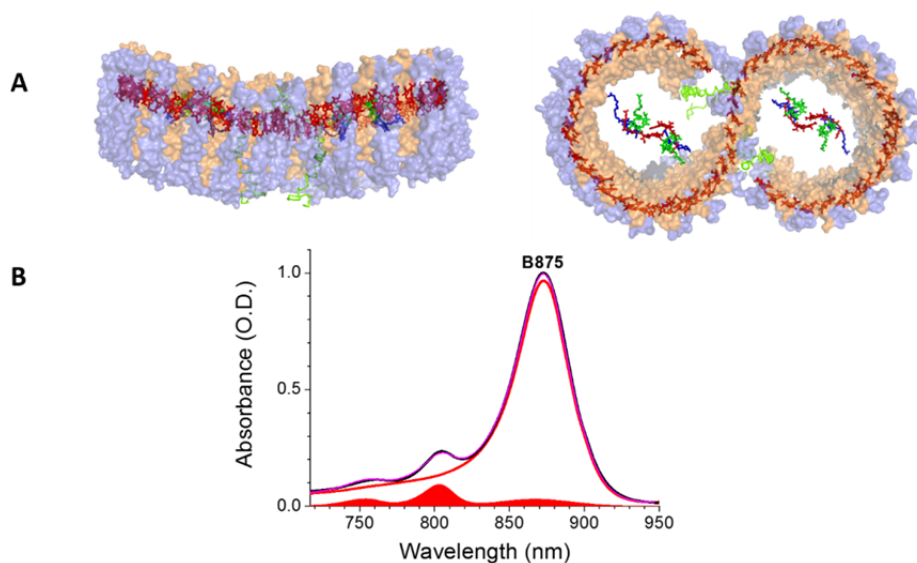


Fig. 1.3. (A) The structure of the RC-LH1-PufX dimer core complex viewed either from the side (left hand side) or from the top (right hand side). To highlight the position of the pigment molecules in the protein, 50% transparency was imposed. The LH1 BChls pigments are coloured in red. For clarity, only the BChl special pair (red), accessory BChl (green) and Bphe (blue) are shown for the RC cofactors. The PufX polypeptide is coloured in light green. (B) Absorption spectra of the RC-LH1-PufX complex (black line) with the properly scaled sum spectrum (pink line) of membrane RC (shaded area) and LH1 (red line) complexes.

In contrast to LH2 absorption spectra, the RC-LH1-PufX core complex from *Rba. sphaeroides* has a single BChl absorbance band peaking at 875 nm, called B875 band (Fig. 1.3 B). The sum spectrum (pink line) verifies that the additional minor peaks seen in the core complex absorption spectrum at ~ 758 nm and ~ 806 nm is exclusively from the RC (red shaded area), see below. These two absorption bands of RC are respectively related to the bacteriopheophytin (traditionally named as H) and to the bacteriochlorophyll monomer (B). The additional band in RC, peaking at 868 nm is related to the special pair (P), which is generally hidden under the LH1 B875 band. These bands related to the RC are more clearly noticeable in Fig. 1.4 B.

It is further worth mentioning that the ratio of the monomeric and dimeric core complex present in the photosynthetic membranes of *Rba. sphaeroides* depends on the type of carotenoid present in the membranes [61], and that the absence of PufX in certain native [53, 58] and mutant [70] complexes results in 16 $\alpha\beta$ -BChl₂ structural elements of LH1 fully encircling a single RC, the planar monomeric core complex RC-LH1.

1.2.1.3. The reaction centre

The purple bacterial RC is a pigment-protein complex where the excitation energy is transferred to chemical energy with quantum yield approaching 1 [71-73]. The RC is also one of the best known structural components of the bacterial PSU along with LH2. The *Rba. sphaeroides* RC was the first to be biochemically purified, from a carotenoid-less LH2-deficient mutant called R-26 [74, 75]. Here a brief outline of the crystal structure of the RC from *Rba. sphaeroides* is presented. These structures were obtained first from the R-26 mutant, later from other mutants, with the resolution refined down to 2.35Å [76-82]. The RC from *Rba. sphaeroides* contains three protein subunits, known as L (light), M (medium), and H (heavy), respectively. As the structures of all purple bacterial RCs are expected to be quite similar, Fig 1.4 A shows the RC structure of *Rhodospseudomonas viridis*. This structure contains eight cofactors, which form 2 potential electron transfer (ET) chains (referred to as A and B) in a nearly C₂ symmetric arrangement: two BChls (P_A, P_B) of the special pair P, two accessory BChls in close proximity to P (B_A, B_B), two bacteriopheophytins (H_A, H_B), and a pair of quinones (Q_A, Q_B) [76, 83]. The absorption spectrum presented in Fig 1.4 B clearly distinguishes three maxima peaking at 758 nm, 806 nm and 868 nm and associated with H, B and P. When P is excited by light (P*), a multi-step ET process is initiated, where an electron is transferred only through the A branch cofactors, and then to Q_B. In the WT RC, the times for ET from P* to H_A to Q_A to Q_B are 3 ps, 200 ps, and 200 μ s, respectively. The transfer from P* to H_A is thought to be via B_A. These processes in RC have been extensively studied, and being the subject of numerous review articles [84-92], they will not be further explained here.

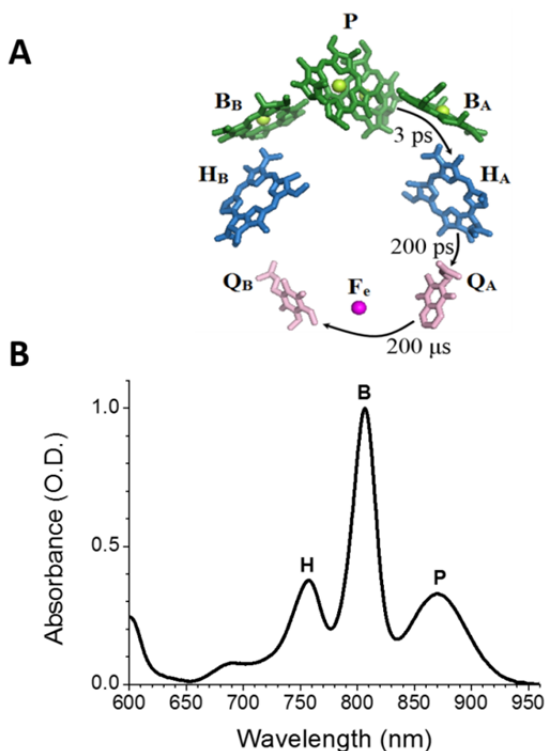


Fig. 1.4. (A) Structure of the photosynthetic RC cofactors of *Rhodospseudomonas viridis*. The electron pathways are indicated with corresponding time constants. The central Mg atoms of the BChl pigments are indicated with circles. (B) Absorption spectrum of the WT RC membranes from *Rba. sphaeroides*. See text for further details.

1.2.2. Adaptation of intracytoplasmic membranes into different levels of light intensities

As detailed in section 1.1, the photosynthetic purple bacteria are anaerobic organisms. Thus they require both light and anoxic conditions for their competitive existence in nature according to the evolution via natural selection, the main biological principle. These conditions are generally met in the anaerobic layers in ponds, lakes and streams [93]. The environmental conditions such as light intensity and its spectral distribution in these habitats vary on a large scale. To ensure effective photosynthesis, the structural composition and the related spectral properties of the bacterial PSU have to be versatile. Recent high resolution atomic force microscopy studies of the ICM of bacteria have revealed variations of the structural organization of PSU that parallel to the growth conditions [30, 94, 95]. In the chromatophores collected from *Rba. sphaeroides* grown under high light intensity (henceforth called high light (HL) adapted membranes), the number of peripheral LH2 complexes available in PSU is relatively small, whereas in low light (LL) adapted chromatophores, which have been harvested from the cells grown

under dim light, the PSU is dominated by the LH2 complexes [95-98]. In some other species of photosynthetic purple bacteria light adaption involves significant modification of spectral properties as well as the structure of the distal antenna [30, 98, 99]. For instance, when grown at lower light intensities and/or lower temperature, a spectral variant of the B800-850 LH2 called the LH3 (B800-820) is synthesized in *Rps. acidophila* [100, 101]. These structural and spectral adaptations allow the bacteria to accommodate to different ecological niches.

A cartoon illustration of the patches of HL and LL adapted chromatophore membranes along with their Q_y electronic absorption spectra, decomposed into their distal and core antenna parts, are presented in Fig.1.5. The general procedure to quantitatively evaluate the ratio of distal and core antenna complexes (LH2 to LH1 ratio or LH2/LH1 for short) from the decomposed spectra is discussed below, see [102, 103] for more specific considerations.

The absorption spectra of the chromatophore samples were fitted with the sum of the absorption spectra of the mutant membranes that contained solely either the peripheral LH2 or the core RC-LH1-PufX complexes in the wavelength range from 700 nm to 950 nm. For a satisfactory fit the component spectra were allowed to shift in wavelength scale and accommodate in intensity scale. The 850 nm band of

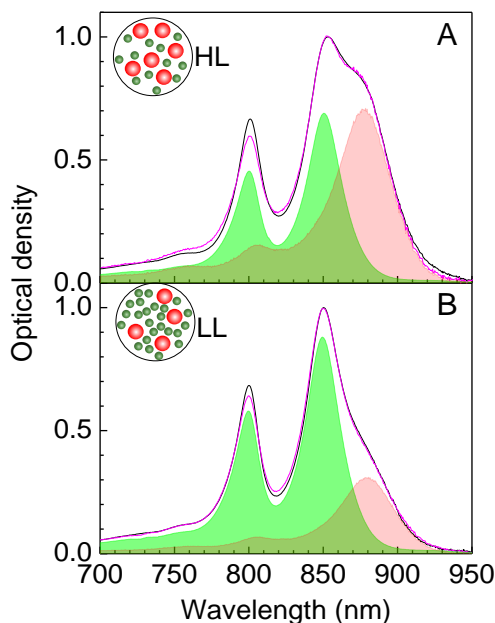


Fig. 1.5. Decomposition of the absorption spectra of the HL (A) and LL (B) adapted WT chromatophores from *Rba. sphaeroides*. Shown in black and pink curves are the measured and simulated absorption spectra, respectively. The fitting sub-spectra of the LH2-only and RC-LH1-PufX-only membranes, correspondingly, are shown in shades of green and red. Identities of the spectral maxima are the same as in Fig 1.1. The insets in panels A and B schematically illustrate the samples. The peripheral and core antenna complexes are respectively distinguished by green and red spheres.

LH2 was fitted more carefully than the 800 nm band owing to the inherent intensity variations in the B800 absorption band of still unknown origin. Once the best fit is achieved, the integrals, i.e. the areas below the fitted curves, of the component spectra were used to evaluate the ratio LH2/LH1. Assuming equal absorption of the BChl chromophores in LH2 and LH1 complexes as well as in RC's and knowing the number of BChls in LH2 (27 [104]), RC-LH1-PufX dimer (56 in LH1 and 4×2 in RC [53, 105]), and RC-LH1-PufX monomer (30 in LH1 and 4 in RC [62]) complexes, the LH2/LH1 ratio was evaluated. In Paper II, the LH2/RC ratio was obtained taking into account the number of RCs per core complex (2 for dimeric, 1 for monomeric case).

1.3. Exciton interpretation of the bacterial spectra

Photosynthesis involves the interaction of light with living matter and the dynamics of the electronically excited quantum states of the pigment-protein complexes [106-109]. Quantum mechanics is thus inevitable for the description of the primary process of photosynthesis. The electronically excited states of the collection of BChl molecules in the peripheral and core complexes are described by the following Hamiltonian:

$$H = \sum_{n=1}^N E_0 |n\rangle\langle n| + \sum_{n=1}^N \sum_{m \neq n} V_{nm} |n\rangle\langle m| \quad (1)$$

Here, each molecule is assumed to be a two-level system consisting of a ground state and a single electronically excited state separated by excitation energy E_0 (also called site energy). A molecule, n , in the electronically excited state is denoted by $|n\rangle$ while all other molecules $1, 2, \dots, n-1, n+1, \dots, N$ are in the electronic ground state. V_{nm} represents the interaction energy between the molecules in excited states located on molecule n and m . This intermolecular interaction is in many cases dominated by the electrostatic interactions between the electrons and nuclei from neighboring molecules. The Coulombic interaction between two molecules n and m in a medium characterized by the dielectric constant ϵ can be described by:

$$V_{nm} = \frac{1}{4\pi\epsilon} \sum \frac{q_n q_m}{r_{nm}}, \quad (2)$$

where r_{nm} is the distance between the electronic and nuclear charges q_n and q_m on both molecules.

It is useful to expand the interaction energy into a power series when the electrostatic interactions are much larger than the exchange interactions, i.e., when the intermolecular distance is large compared to the molecular size. (Although this latter assumption has limited reliance for B850 and B875 assemblies of BChls in LH2 and LH1 complexes, respectively [110, 111], the simplified model presented here is sufficient for qualitative understanding of the under-

lying processes studied in this work.) In the multipole expansion, provided that one is dealing with the uncharged molecules, the interaction energy can be approximated with the dipole-dipole term as described below:

$$V_{nm} = \frac{1}{4\pi\epsilon} \frac{|\mu_n||\mu_m|}{r_{nm}^3} \mathcal{K}_{nm}, \quad \mathcal{K}_{nm} = [(\hat{\mu}_n \cdot \hat{\mu}_m) - 3(\hat{\mu}_n \cdot \hat{r}_{nm})(\hat{\mu}_m \cdot \hat{r}_{nm})] \quad (3)$$

Here, $\hat{\mu}$ is the transition-dipole moment vector of the molecules. r_{nm} is the distance between the transition dipoles $\hat{\mu}_n$ and $\hat{\mu}_m$. For a complete description the reader is referred to [51].

As a consequence of the intermolecular interaction, the eigenfunctions of the Hamiltonian of Eq. 1 are given as the linear combinations of the localized wavefunctions of the individual pigments, commonly known as Frenkel (molecular) exciton wavefunctions:

$$|k\rangle = \frac{1}{\sqrt{N}} \sum_{n=1}^N e^{i2\pi k \frac{n}{N}} |n\rangle, \quad (k = 0, \dots, N - 1) \quad (4)$$

The exciton wavefunctions are thus delocalized over all sites of the molecular assembly.

In Eq. 1 the site energy, E_0 for all pigments was taken the same. However in reality the variations in the local electrostatic interactions within the protein give rise to static disorder in the site energies of the pigments. This variation in the site energy is represented by a random shift ΔE_n and is referred to as diagonal disorder. Variations of the pigment-pigment interaction, which may be static or dynamic, are represented by ΔV_{nm} . Correspondingly this disorder is referred to as off-diagonal disorder. Combining the diagonal and off-diagonal disorder to Eq. 1, the Hamiltonian modifies as:

$$H = \sum_{n=1}^N (E_0 + \Delta E_n) |n\rangle\langle n| + \sum_{n=1}^N \sum_{m \neq n} (V_{nm} + \Delta V_{nm}) |n\rangle\langle m|. \quad (5)$$

Both diagonal and off-diagonal disorders disturb excitons causing spatial localization of the exciton wavefunctions. Qualitatively, in case of diagonal disorder, the character of the electronically excited state depends on the ratio of the relative magnitude of the interaction energy V and the site energy difference ΔE . When the coupling is weak, $\left| \frac{V}{\Delta E} \right| \ll 1$, the excited state wavefunctions are mainly localised on individual pigments and the description in terms of the site representation, $|n\rangle$, is a good approximation. In the opposite strong coupling limit, $\left| \frac{V}{\Delta E} \right| \gg 1$, delocalized exciton is a better representation of the physical situation and Eq. 4 holds. It has to be emphasized here that the energy transfer between the pigments in the weak coupling limit can be visualized as a diffusive hopping process, also called incoherent energy transfer, whereas in the strong coupling case, it occurs in a wave like manner, being referred to as coherent energy transfer.

Let's consider the two separate (i.e., weakly coupled) assemblies of the BChl pigments, B800 and B850, in LH2 (see Fig. 1.2) as representative examples. In the B800 ring, the nearest-neighbor interaction energy, V , has been estimated to be $\sim 24 \text{ cm}^{-1}$ and the variation (standard deviation) of the site energies, estimated from the inhomogeneously broadened ensemble spectrum is $\sim 180 \text{ cm}^{-1}$ [52]. This results a $\left| \frac{V}{\Delta E} \right|$ ratio of about ~ 0.1 , consequently the respective spectrum can be related to the optical excitation of weakly coupled B800 pigments that are strongly localised on individual BChl pigments [52]. The estimated numbers of V and ΔE (respectively 300 and 200 cm^{-1}) for the B850 molecules give $\left| \frac{V}{\Delta E} \right| > 1$ and suggest that the excitation energy is delocalized among the pigment [112-117]

In order to provide an insight into the general features of the LH2 (B850) and LH1 (B875) exciton spectra in Q_y range, the disorders are for simplicity assumed to be zero, i.e. $\Delta E = 0$ and $\Delta V = 0$. Starting with such idealised B850, the interaction term, V_{nm} , in Eq. 1 leads to a splitting (Davydov splitting [118]) of the initially degenerated excited states of the 18 BChl molecules within the B850 ring into an exciton band where the 18 exciton eigenstates, are spread over $\sim 1200 \text{ cm}^{-1}$ (Fig 1.2 B) [99, 119-121]. These excitonic states have been indexed from $k = 0$, $k = \pm 1$ to $k = \pm 8$, $k = 9$, where the \pm indicate energetically degenerate states having mutual orthogonal orientation of the transition dipole moments. Due to the circular arrangement of the pigments in the LH2, of the 18 exciton states, only $k = 0$, $k = \pm 1$ and $k = \pm 8$, $k = 9$ have a non-vanishing transition-dipole moment [52]. Among these possible 6 exciton states, due to the head-to-tail arrangement of the transition dipole moments within an individual dimeric protein subunit and nearly in the B850 ring plane, almost all the oscillator strength is concentrated on the $k = \pm 1$ region, being also responsible for the characteristic B850 absorption band of LH2. The upper exciton state $k = \pm 8$ that gives rise to a faint absorption ($< 3\%$ of the total oscillator strength) is partly overlapping with the B800 band.

The formation of the LH1 spectra in core complexes is similar. However, apart from greater number of exciton states, important differences of the excitonic properties appear either due to PufX breaking the perfect circular symmetry of the core complex or because of the monomeric and dimeric build-up of the core complexes [122]. In the full-ring monomeric core complex such as found in chromatophores from *R. rubrum*, the closely doubly degenerate energy levels are present in the B875 excitonic band, qualitatively like in B850 of LH2. This structure is further disturbed in the core complexes of *Rba. sphaeroides* as a consequence of introducing PufX into monomeric and dimeric core complexes. While in all the core complexes the major contribution to the oscillator strength is carried by the $k = \pm 1$ exciton states, in case of the core complexes of reduced symmetry the non-degenerate exciton state $k = 0$ acquires greater significance.

Exciton as originally solid state phenomenon [123, 124] has usually been considered in relation with highly ordered materials studied at low tempera-

tures. Photosynthetic excitons were discussed in the literature over more than half century before being firmly established in late 1990s. Present evidence of photosynthetic excitons is massive. Although the role of various low-temperature spectroscopies (in combination with structural and theoretical studies) in this success have been instrumental, the existing data leave no doubt that photosynthetic excitons survive high physiological temperatures. Naturally, due to strong dynamic (conformational) disorder prevailing at high temperatures, these excitons are more localized than those at cryogenic temperatures [52, 125-128].

1.4. Excitation energy transfer and trapping process in the photosynthetic unit

1.4.1. Excitation energy transfer – A brief theoretical overview

Being acquainted with the structure-function information, spectroscopic properties, and the electronic excitations of the individual pigment-protein complexes, the next step towards an understanding of the PSU functioning is to describe the excitation energy transfer (EET) processes between the individual pigment-protein complexes. Qualitative understanding of these processes can be obtained by the Förster resonance energy transfer (FRET) model [129]. However, as will be briefly detailed below, one should keep in mind that the classical Förster mechanism is insufficient to account for the many energy transfer steps encountered in the PSU and it generally fails to explain the measured energy transfer rates.

Figure 1.6 illustrates the energy transfer between a donor and an acceptor pigment. Initially the donor pigment is in the electronically excited state, D^* and the acceptor is in the electronic ground state, A . This state is denoted by D^*A . As result of a Columbic interaction, V an excitation energy transfer occurs between the pigments leading the donor to the ground state and the acceptor to the excited state. This final state is named as DA^* .

According to the Fermi's Golden Rule, the transfer rate between any two quantum states with energies E_A and E_D is given by,

$$k_{DA} = \frac{2\pi}{\hbar} V_{DA}^2 \delta(E_D - E_A), \quad (6)$$

where V_{DA} is the interaction energy between the two states. The term $\delta(E_D - E_A)$, called the delta function ensures energy conservation for the particular energy transfer process. In condensed phases, including biological samples, due to the vibrational motion of the surrounding environment at finite temperature, this last term is replaced by a spectral overlap integral and the rate Eq. 6 should read as,

$$k_{DA} = \frac{2\pi}{\hbar} V_{DA}^2 \int_{-\infty}^{+\infty} dE S_D(E) S_A(E) \quad (7)$$

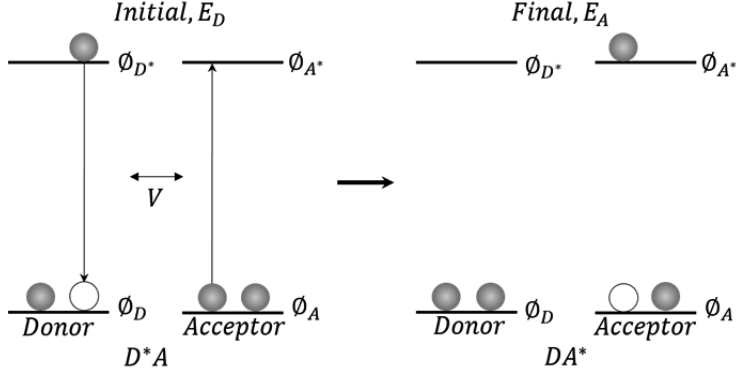


Fig. 1.6. The EET between an initially excited donor pigment, D^* , and an initially unexcited acceptor pigment, A , through interaction energy V . ϕ_D , ϕ_A , and ϕ_{D^*} , ϕ_{A^*} represent the ground state and the excited state orbitals of the donor and acceptor pigments respectively. The downward arrow indicates a non-radiative relaxation of the donor pigment into the ground state that induces an acceptor pigment into the excited state (upward arrow) through the inter-molecular coupling V . See text for further explanation.

In Eq. 7, S_D and S_A are the normalized emission and absorption spectrum of the donor and the acceptor pigments, respectively. When the electrostatic interactions are much larger than the exchange interactions, the interaction energy can be approximated with the dipole-dipole term $\frac{1}{4\pi\epsilon} \frac{|\mu_D||\mu_A|}{r_{DA}^3} \mathcal{K}_{DA}$, as given by Eq. 3. Inserting such an interaction energy into Eq. 7 yield the well-known formula for Förster resonance energy transfer (FRET),

$$k_{DA} = \frac{1}{8\pi\hbar\epsilon^2} \frac{\mu_D^2 \mu_A^2 \mathcal{K}_{DA}^2}{r_{DA}^6} \int_{-\infty}^{+\infty} dE S_D(E) S_A(E) \quad (8)$$

Here the orientation factor, \mathcal{K}_{DA} is often averaged over all possible directions of $\hat{\mu}_D$ and $\hat{\mu}_A$ to give $\mathcal{K}_{DA}^2 = 2/3$, which simplifies the Eq. 8 into

$$k_{DA} = \frac{1}{12\pi\hbar\epsilon^2} \frac{\mu_D^2 \mu_A^2}{r_{DA}^6} \int_{-\infty}^{+\infty} dE S_D(E) S_A(E) \quad (9)$$

In contrast to excitonic energy transfer described in section 1.3, the Förster resonance energy transfer rate is formulated based on the assumption of weak coupling limit, i.e. the interaction energy, V , between the participating pigment molecules is smaller compared to the difference in site energy, ΔE . Thus in case of FRET, the molecules can be thought of as essentially independent entities, while in case of excitons, the donor and acceptor electronic states mix strongly to produce new, delocalized states. If the interaction energy is approximated with the dipole-dipole term, the matrix element of the interaction between the donor and acceptor molecule, depends on their mutual distance, r , as $1/r^3$. How-

ever, as seen above, upon squaring the matrix element of the interaction between the pigment molecules, the FRET rate depends on the donor acceptor separation distance as $1/r^6$.

Despite relative success in explaining the many aspects of EET [24, 108], none of the relevant energy transfer steps can be completely explained by the conventional Förster mechanism. The fundamental pre-requisite of FRET is that the length of the transition dipole moments of donor and acceptor agents has to be small with respect to the mutual distance of the participating pigment molecules. This precondition is, for example, not fulfilled for the assembly of B850 molecules, as they form a collective excitonic state that is delocalised over a large part of the B850 ring. In other words, in case of the EET from a B800 molecule to the B850 ring, due to the excitonic effect the acceptor ensemble is large with respect to the intermolecular distance between the B800 molecule and the B850 ring. Consequently the Förster approach fails and a more sophisticated approach is required to characterize EET process [130]. In order to quantitatively describe the EET in the PSU other theoretical approaches have been applied, including generalized Förster resonance energy transfer [106, 110, 131], multichromophoric Förster resonance energy transfer [132, 133], Redfield theory [134-136] and electron exchange (Dexter) mechanism [50, 137].

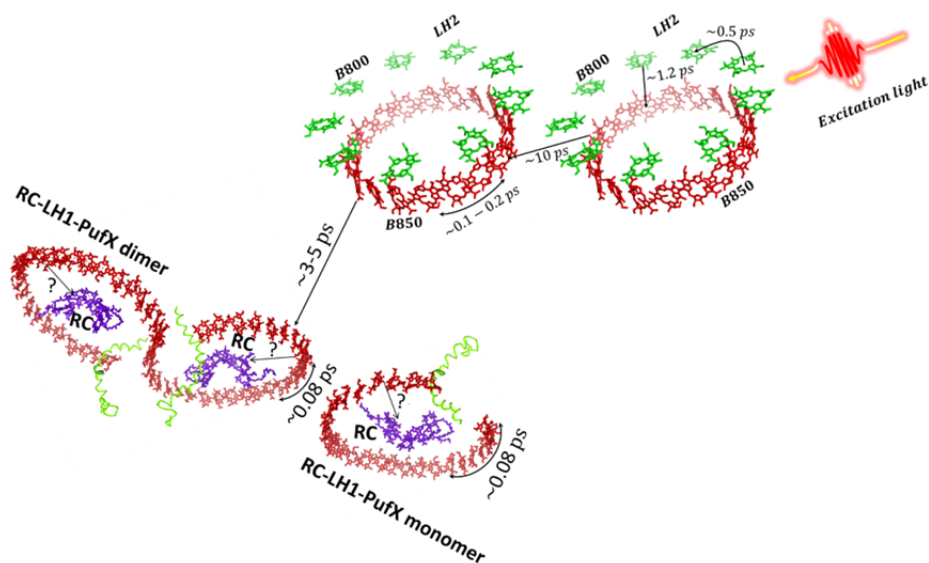


Fig. 1.7. Illustration of the ultrafast EET processes following excitation by light beam in the PSU of a photosynthetic purple bacterium allowing the simultaneous presence of monomeric and dimeric core complexes. Shown for simplicity is just pigment content of the respective pigment-protein complexes. The EET times are presented in picoseconds. The question mark indicates the processes/times where the present knowledge is most ambiguous and requires additional studies.

We conclude this section with Fig. 1.7 that summarizes the different experimentally observed exciton migration pathways and times of EET within the PSU of photosynthetic purple bacteria. Different tracks of excitation energy transfer include following energetically ‘downhill’ steps (see also Fig. 1.1): B800 (LH2) → B800 (LH2), B800 (LH2) → B850 (LH2), B850 (LH2) → B850 (LH2), B850 (LH2) → B875 (LH1), B875 (LH1) → RC.

As seen, the observed EET times clearly divide into two groups – those between the closely coupled pigments within the ring antenna systems and those between the not so strongly coupled pigments in different complexes or different rings. The former times, which characterize the coherent exciton transfer mechanism, are usually an order of magnitude shorter than the latter, which reflect non-coherent EET. As seen in Fig. 1.7, where the literature data for *Rba. sphaeroides* species have been gathered, the energy is transferred from one BChl to another within the B800, B850, and B875 rings, respectively, in about 0.5 ps, 0.1–0.2 ps, and 0.08 ps. The energy reaches the B850 ring from the B800 ring in 1.2 ps at low temperatures and in 0.7 ps at ambient temperatures. The further energy transfer steps B850 (LH2) → B875 (LH1), B850 (LH2) → B875 (LH1), and B875 (LH1) → RC occur in 1–10 ps, 3–5 ps, and 55 ps, respectively [108, 138-141]. The energy transfer data for the core complexes distinguishing between their monomeric and dimeric forms are absent to the best of our knowledge. The primary charge separation usually occurs in about 3 ps. However, this time can be significantly elongated by genetic engineering the RCs. For example, in the genetically modified YM210W RC, where the native tyrosine residue is replaced by tryptophan at the site M210, it becomes about 60 ps.

It should be emphasised that most of the above times have been determined either in isolated complexes or in genetically modified membranes comprising just one type of protein complexes (LH1, LH2 or RC). The data about the EET and trapping times in intact chromatophore membranes of photosynthetic bacteria available so far is rather incomplete. This is mainly because of limited information about the complex structure of the PSU that also depends on multiple external factors, as already discussed. The exciton trapping times determined as the mean fluorescence lifetime in the well-defined WT and genetically modified chromatophores as well as in sole core complexes of *Rba. sphaeroides* have been measured during the course of this thesis.

1.4.2. Factors that influence the energy trapping time in the core complex

The overall exciton energy trapping time in WT *Rba. sphaeroides* chromatophores with active RCs was determined as 68–82 ps [142]. In the very same work, it was established that the trapping time of antenna excitons depends on the functional state of RC, which can exist either in an ‘open’(active) or in a ‘closed’ (inactive) state. In the ‘open’ state, the RC special pair is reduced and

able to promptly utilize the special pair excitation towards a charge separation. This state hence results in a short trapping time. “Closing” of the RC is here interpreted as photo-induced oxidation of the special pair. The oxidized RC is unable to further utilize photo-excitations, resulting in an elongated fluorescence lifetime. The RC remains “closed” until it is reduced by an uptake of an electron. In normal conditions this will take tens to hundreds of millisecond. The extent of closed RCs in PSU thus depends on the intensity of the illuminating light (i. e., the supply frequency of the absorbed photons). Although the RC cannot photo-chemically utilize antenna excitons during the “closed” state, it can still quench them rather effectively by non-radiative decay mechanisms [143]. This determines that the lifetime of excitons in chromatophores with inactive RCs is always shorter than that in isolated LH complexes.

Referring to the principal findings from this study, the next significant factor that influence the trapping time is the structural organization of the core complex (as described in sections 4.2 and 4.3). The dimeric core complex is more efficient in excitation energy trapping compared to the monomeric core complex. The trapping time in PSU additionally depends on the number of peripheral antenna complexes that are present in the chromatophore, which duly depends on the growth light intensity (section 4.1).

1.4.3. Kinetic model of exciton population dynamics in the photosynthetic unit of purple bacteria

This section details the kinetic model that has been used in this study (section 4.1 and 4.2) to describe the population dynamics of excited LH2 and LH1 chlorophylls in the PSU of purple bacteria. This analysis is required in order to comprehend the experimentally observed stationary and time resolved fluorescence results. The model is presented in Fig. 1.8. It defines a mathematical relation between the ‘apparent’ rate constants, γ , each characterizing an exponential component of the observed multi-exponential fluorescence decay, and the ‘microscopic’ rate constants, k , each characterizing a specific kinetic pathway.

The system of kinetic equations corresponding to the basic model shown in the right side of Fig.1.8 is:

$$\begin{aligned} \frac{dA}{dt} &= -k_1 A - k_{loss}^{LH2} A + k_{-1} B \\ \frac{dB}{dt} &= k_1 A - k_1 B - k_2^{o,c} B \end{aligned} \quad (10)$$

where $A(t)$ marks the population of the B850 excitons in LH2, $B(t)$ that of the B880 excitons in LH1, and $k_2^{o,c}$ stands either for k_2^o or for k_2^c , depending on the state of RCs (see below).

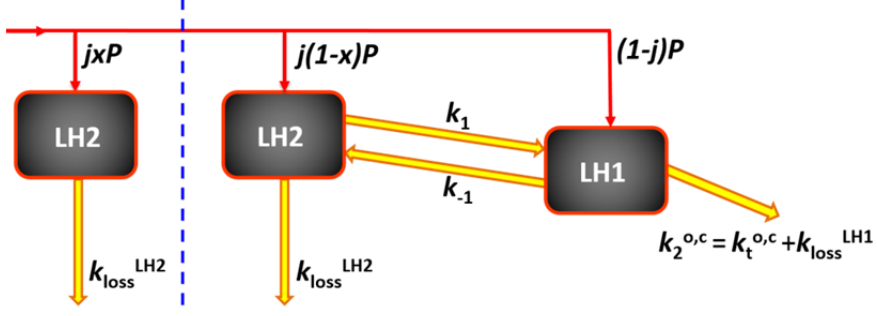


Fig. 1.8. Kinetic scheme of the exciton population dynamics in PSU of purple bacteria. The basic scheme (right from the vertical dotted demarcation line) comprises functionally connected LH2 and LH1 compartments. An additional compartment (left from dotted line) applied in the extended model represents functionally unconnected or poorly connected LH2 pool. The total absorbed power is denoted by P . Red arrows illustrate the branching of the absorbed power between the compartments governed by the factors j and x , where $0 \leq j, x \leq 1$. The factor x represents a fraction of unconnected LH2 units. Each kinetic pathway is characterized by a rate constant.

The solution of Eq.10 describing the observed decay curves is given by

$$\begin{aligned} A(t) &= a_1 e^{-\gamma_1 t} + a_2 e^{-\gamma_2 t}, \\ B(t) &= b_1 e^{-\gamma_1 t} + b_2 e^{-\gamma_2 t}, \end{aligned} \quad (11)$$

where γ_1 and γ_2 are the apparent rate constants, and a_1 , a_2 , b_1 , and b_2 are the time-independent coefficients that depend on the microscopic rate constants k_1 , $k_{\text{loss}}^{\text{LH2}}$, k_{-1} , $k_2^{o,c}$ as well as the initial populations of excitations, $A(0)$ and $B(0)$. The factors $\exp(-\gamma_1 t)$ and $\exp(-\gamma_2 t)$ are assumed to be zero for $t < 0$.

According to this basic model, the apparent rate constants γ_1 (the inverse of the spectrally dependent lifetimes measured at ≤ 850 nm) and γ_2 (the inverse of spectrally dependent lifetimes at ≥ 880 nm), and the microscopic rate constants are connected as follows [144]:

$$\begin{aligned} \gamma_1 &= \frac{1}{2} \left[(k_{\text{loss}}^{\text{LH2}} + k_1 + k_{-1} + k_2^{o,c}) \right. \\ &\quad \left. + \sqrt{(k_{\text{loss}}^{\text{LH2}} + k_1 - k_{-1} - k_2^{o,c})^2 + 4k_1 k_{-1}} \right] \\ \gamma_2 &= \frac{1}{2} \left[(k_{\text{loss}}^{\text{LH2}} + k_1 + k_{-1} + k_2^{o,c}) \right. \\ &\quad \left. - \sqrt{(k_{\text{loss}}^{\text{LH2}} + k_1 - k_{-1} - k_2^{o,c})^2 + 4k_1 k_{-1}} \right] \end{aligned} \quad (12)$$

In Eq. 12, k_1 and k_{-1} are, respectively, the forward and backward energy transfer rate constants between the LH2 and LH1 compartments; $k_{\text{loss}}^{\text{LH2}}$ is the total rate constant of the excitation loss from the LH2 compartment apart from the transfer of excitation energy to LH1, and $k_2^{o,c}$, the decay rate constants of LH1 excitons in case of open (k_2^o) and closed (k_2^c) RCs. For convenience, we have also defined that $k_2^{o,c}$ is a sum of the trapping rate constants, $k_t^{o,c}$, by open or closed RCs, and $k_{\text{loss}}^{\text{LH1}}$, the rate constant of any other kind of decay of LH1 excitons apart from their transfer to RC, i.e.:

$$k_2^{o,c} = k_t^{o,c} + k_{\text{loss}}^{\text{LH1}} \quad (13)$$

Under thermal equilibrium, the forward (LH2 \rightarrow LH1) and backward (LH1 \rightarrow LH2) energy transfer rates, k_1 and k_{-1} (assumed to be independent from the RC state) are related to each other via the Boltzmann factor. The equilibrium constant defined as $K = k_1/k_{-1}$ is given:

$$K = \frac{k_1}{k_{-1}} = \frac{N_{\text{LH1}}}{N_{\text{LH2}}} e^{-\frac{\Delta E}{k_B T}} \quad (14)$$

where LH1/LH2 is the ratio of the core and peripheral antenna complexes, N_{LH1} and N_{LH2} are the numbers of the BChl chromophores in the B875 and B850 arrangements in LH1 and LH2, respectively, and ΔE is the energy gap between the lowest-energy exciton states of LH1 and LH2. From the structure of light harvesting antennas of *Rba. sphaeroides* with PufX protein, it is known that $N_{\text{LH2}} = 18$ while N_{LH1} can be either 30 or 56 respectively in case of monomeric and dimeric core antenna complex (see section 1.2.1.2). ΔE is for simplicity defined as the difference between the LH1 and LH2 absorption maxima, obtained by the decomposition of the absorption spectra of the membrane samples, as described in section 1.2.2.

The steady state excited state populations can be deduced from the system of kinetic equations

$$\begin{aligned} (k_1 + k_{\text{loss}}^{\text{LH2}})A - k_{-1}B &= jP \\ -k_1A + (k_{-1} + k_2)B &= (1-j)P, \end{aligned} \quad (15)$$

where P is the excitation rate that is proportional to the power of incident light, and j and $(1-j)$ describe the branching of excitation between the LH2 and LH1 compartments, respectively. By solving this system of equations the steady state fluorescence yield ratio, F850/F880, can be expressed as

$$\frac{F_{850}}{F_{880}} = \frac{A}{B} = \frac{k_{-1} + jk_2}{k_1 + k_{\text{loss}}^{\text{LH2}}(1-j)}. \quad (16)$$

Once the experimentally observable parameters, such as γ_1 , γ_2 , $k_{\text{loss}}^{\text{LH2}}$, $k_{\text{loss}}^{\text{LH1}}$, j , and F850/F880, are available, all the relevant microscopic rate constants can

be determined iteratively using Eqs. 12–14 and 16 to harmonize the calculated and experimental fluorescence yields and lifetimes. The decay rates $k_{\text{loss}}^{\text{LH2}}$, $k_{\text{loss}}^{\text{LH1}}$ were obtained by taking the reciprocal of the experimentally measured fluorescence decay time of LH2-only and LH1-only membrane respectively. The branching of excitation between the LH2 and LH1 compartments that occur due to overlap of their absorption spectra at the excitation wavelength (see Fig 1.5). The value of branching ratio, j , for 800 nm excitation for the studied samples were obtained from their absorption spectra as in [103]. An effect of excitation de-trapping from RC [145-148] on the LH2/LH1 branching ratio is small [103] and has been ignored. LH1 is then the only complex that absorbs under 915 nm excitation, i.e. $j = 0$ in this case. The relative contributions of the F850 (i.e. fluorescence related to B850) and F880 (fluorescence related to B880) components were obtained by de-convoluting the stationary fluorescence spectra of the samples in the similar way as in Fig 1.5 but in energy scale. Thus the ratio of the integrated fluorescence yields of the LH2 and LH1 sub-bands, F850/F880 were obtained. More specific prerequisites considered during the calculations can be seen in papers I and II.

In order to evaluate the relative fraction of the unconnected or poorly connected LH2s, the basic kinetic model were extended by adding the left part of Fig. 1.8. In this case, the steady state excited state populations in the presence of disconnected or poorly connected LH2s can be extracted from the following system of kinetic equations:

$$\begin{aligned} k_{\text{loss}}^{\text{LH2}}C &= jxP, \\ (k_1 + k_{\text{loss}}^{\text{LH2}})A - k_{-1}B &= j(1-x)P, \\ -k_1A + (k_{-1} + k_2)B &= (1-j)P, \end{aligned} \quad (17)$$

where A and C are the populations of excited LH2 complexes that are, respectively, connected and disconnected with the core complexes, B is the population of excited LH1 complexes, P is the excitation rate that is proportional to the power of incident light, and x is the relative fraction of disconnected LH2s ($0 < x < 1$). The system of equations 17 can be solved for A , B and C , for instance, by the method of determinants. The steady state fluorescence yield ratio is then given by:

$$\frac{F_{850}}{F_{880}} = \frac{A+C}{B} = \frac{k_{-1} + jk_2(1+xk_1/k_{\text{loss}}^{\text{LH2}})}{k_1(1-jx) + k_{\text{loss}}^{\text{LH2}}(1-j)}. \quad (18)$$

1.4.4. Quantum efficiency of energy trapping

The quantum efficiency of the primary stage of photosynthesis, defined as the probability that an absorbed photon leads to the charge separation in a RC [149], can be calculated as the ratio of the trapping rate of the LH1 excitons by open RCs divided by P , the rate of excitation by the incoming light. Under steady state excitation the trapping rate by open RCs is given by ($k_2^o -$

$k_{loss}^{LH1})B$, where $(k_2^o - k_{loss}^{LH1})$ is the trapping rate constant in case of open RC and B is the steady state population of LH1 excitons. By expressing B from Eq. 15 through the rate constants the equation for the quantum efficiency takes the form:

$$\eta = \frac{(k_2^o - k_{loss}^{LH1})B}{P} = (k_2^o - k_{loss}^{LH1}) \left(\frac{1 + k_{loss}^{LH2}(1-j)/k_1}{k_2^o + k_{loss}^{LH2}(1/K + k_2^o/k_1)} \right) \quad (19)$$

In case of $k_{loss}^{LH2} = 0$, Eq. 19 reduces to $\eta = (k_2^o - k_{loss}^{LH1})/k_2^o$ that accounts only the population losses in LH1 [145-148].

Using the microscopic rate constants evaluated in section 1.4.3, one can easily calculate the quantum efficiency of active photosynthesis by Eq. 19. In the presence of unconnected or ill-connected LH2s the quantum efficiency can be calculated using the following equation:

$$\eta = (k_2^o - k_{loss}^{LH1}) \frac{1 - jx + k_{loss}^{LH2}(1-j)/k_1}{k_2^o + k_{loss}^{LH2}(1/K + k_2^o/k_1)} \quad (20)$$

By expanding Eq. 20 to the Taylor series by k_{loss}^{LH2} and keeping only the first order term the quantum efficiency can be approximated as:

$$\eta = \frac{(k_2^o - k_{loss}^{LH1})}{k_2^o} \left[1 - jx - k_{loss}^{LH2} \left(\frac{j(1-x)}{k_1} + \frac{1-jx}{k_2^o K} \right) \right], \quad (21)$$

where the reduction in efficiency due to disconnected ($x > 0$) or “leaking” ($k_{loss}^{LH2} > 0$) LH2 complexes is explicit. A calculation by the approximate Eq. 21 using typical parameters from this study revealed less than 2% difference compared with that by exact Eq. 20.

1.5. Steady state and picosecond time resolved fluorescence spectroscopy as the method to study primary processes of photosynthesis

Optical methods have contributed extensively in gaining insight in the molecular mechanisms of photosynthesis over at least the last century. In view of the key role of the fluorescing pigment chromophores in photosynthesis, optical methods will certainly continue to enlighten the photosynthetic research. The main experimental methodology that has been used during the course of this thesis was based on fluorescence. Fluorescence emission occurs when an excited molecule decays spontaneously to the ground state, if the radiative transition occurs between electronic states of the same spin. As mentioned in section 1.1, the main probe in this study was native chromophores from a photosynthetic purple bacterium, *Rba. sphaeroides*, either present in the chromato-

phore or in the sole constituent transmembrane protein complexes. It has long been observed that the fluorescence either from chlorophylls or bacteriochlorophylls, a waste when assessed from the point of view of photosynthesis efficiency, provides useful evidence of the mechanisms and dynamics of the primary events in photosynthesis. Thus, using fluorescence as the carrier of information, optical methods provide the possibility of non-invasive measurement of photosynthetic systems, as this information is in principle extracted without interfering with the sample's physiology. The recorded fluorescence from the pigment molecules may have been excited by the photon absorption directly, received its excitation energy by transfer from other pigment molecules or it may be excited by the return of excitation from the traps causing a delayed fluorescence. Time-resolved measurement can be used to elucidate these processes in many cases. The steady-state measurements also provide useful guides to investigating and interpreting the excited state relaxation, nevertheless, it averages the time-dependent behaviour. Both of these experimental approaches have been extensively used in this study, as will be detailed in section 3.3.

2. RESEARCH OBJECTIVES

This thesis explores the primary light harvesting processes in bacterial photosynthesis on the example of a photosynthetic non-sulphur purple bacterium *Rba. sphaeroides*. The photosynthetic apparatus of this bacterium has been extensively studied over the last 5 decades using biochemical, genetic engineering, molecular and structural biology, and spectroscopic methods, which also determines its prominent standing as one of the favorite model systems in the field. However, while our knowledge of the structure and function of each and every component of PSU of this bacterium is extensive, there is still much we do not fully understand in its integral (ultrastructural) functioning as well as in the dynamics of the respective processes. Recent advances in atomic force microscopy combined with innovative synthetic biochemistry have provided evidence for nanoscale structural adaptation of photosynthetic membranes in response to changing their habitats. Examples include mutable stoichiometry of the LH and RC complexes with the light intensity experienced during the membrane development as well as varying architecture of the protein complexes such as dimeric and monomeric core complexes. Therefore, this work addressed some of the central unresolved issues, concerning the nanoscale structural constraints for the ultrafast excitation energy migration and trapping in photosynthetic membranes of bacteria. The main aims of this work can be formulated as follows:

- ✓ To find out how the peripheral antenna size (the relative number of peripheral antenna complexes per core complexes) influence the rates of energy migration towards the RC traps and the efficiency of charge separation at the RCs.
- ✓ To investigate the impact of the monomeric/dimeric structural organization of the core complex on the energy transfer rates and on the efficiency of trapping of antenna excitons.
- ✓ To elucidate the spectral and kinetic changes accompanying the assembly of the LH1 complex with the RC complex into monomeric or/and dimeric core complexes.

In order to solve these problems, the chromatophores extracted from several mutant species of purple bacteria *Rba. sphaeroides* grown under various light conditions were interrogated with a combination of optical absorption, steady state and time resolved fluorescence spectroscopy as detailed in section 3.3. The data were analysed as specified in section 3.4 using the models described in section 1.4.3. The results discussed in section 4 imply a robust photosynthetic apparatus that functions surprisingly effectively under a wide variety of conditions.

3. EXPERIMENTAL

3.1. Samples

The spectroscopic measurement performed in this thesis is either on the ICM or solely on the purified pigment-protein complexes (LHs and RCs) extracted exclusively from the photosynthetic purple bacterium *Rba. sphaeroides*. The cultivation, isolation and purification of these samples were carried out by the laboratories of two collaboration partners: Prof. C. Neil Hunter, University of Sheffield and Dr. Mike Jones, University of Bristol. The order of the samples detailed below is according to the publications i.e. the samples employed in paper I, described first and so on. Table 3.1 outlines complete set of the samples studied along with the buffers and detergent used in their preparation for the measurements.

Table 3.1. The list of buffers and detergents used for the preparation of the samples.¹⁾

Sample	Buffer	Detergent
WT chromatophore	20 mM TRIS ²⁾ pH 7.8	Nil
pseudo WT green chromatophore	20 mM HEPES ³⁾ pH 7.5, 5 mM EDTA ⁴⁾	Nil
mLH2	20 mM HEPES pH 7.5	Nil
mLH1	10 mM TRIS-HCl pH 7.9, 1mM EDTA	Nil
iLH1	10 mM TRIS-HCl pH 7.9, 1mM EDTA	3 mM DHPC ⁵⁾
mRC-LH1	10 mM HEPES pH 7.8, 1mM EDTA	Nil
iRC-LH1	10 mM TRIS-HCl pH 7.9, 1mM EDTA	3 mM DHPC
mRC-LH1-PufX	20 mM HEPES pH 7.8	Nil
iRC-LH1-PufX	20 mM HEPES pH 7.8	0.03% β -DDM ⁶⁾
mYM210W	20 mM TRIS pH 7.8	Nil
iYM210W	20 mM TRIS pH 7.8	0.1% LDAO ⁷⁾

¹⁾ m/i denotes membranes embedded or detergent isolated complexes, respectively.

²⁾ TRIS: Tris(hydroxymethyl)amino methane.

³⁾ HEPES: N-(2-hydroxyethyl) piperazine-N'-(2-ethanesulfonic acid).

⁴⁾ EDTA: Ethylenediaminetetraacetic acid.

⁵⁾ DHPC: 1,2-diheptanoyl-sn-glycero-3-phosphatidylcholine.

⁶⁾ β -DDM : N-dodecyl- β -D-maltoside.

⁷⁾ LDAO: Lauryldimethylamine-N-oxide.

The gene expression for photosynthesis complexes in the WT *Rba. sphaeroides* strain 2.4.1 is dependent upon oxygen levels and light intensity during the growth of the bacterium, with full expression reached under anaerobic conditions and under low light intensity [150, 151]. The WT chromatophore samples used in paper I were prepared according to the method described in [152] from the strain 2.4.1 grown anaerobically using the growth light intensities between 100 $\mu\text{E}/\text{m}^2/\text{s}$ and 1500 $\mu\text{E}/\text{m}^2/\text{s}$. Following the cell disruption by French pressing the cell extracts were loaded onto 15%/40% (w/w) sucrose step gradients and centrifuged for 10 hours at 27,000 rpm. Each intracytoplasmic membrane fraction was harvested from the 15%/40% interface and concentrated by centrifugation.

The chromatophores for paper II were prepared under semi-aerobic conditions in an orbital shaker incubator, as described in [153] either from the strain DPF2G[pRKEH] or DPF2G[pRKEHX Δ 12] that contain respectively dimeric or monomeric core complexes together with controlled high or low LH2 contents. The LH2/LH1 ratio is controlled by changing the degree of aeration of the culture; a high degree of aeration produced a low LH2/LH1 ratio whereas a low degree of aeration formed a high LH2/LH1 ratio [154]. Both of the strain, DPF2G[pRKEH] and DPF2G[pRKEHX Δ 12], were genetically manipulated by deleting the carotenoid D in the carotenoid biosynthesis pathway. This mutation results a green coloration of cultures rather than the usual red observed under semi-aerobic conditions and hereafter they referred as ‘pseudo WT green chromatophores’. Furthermore, this mutation ensures a higher core dimer/monomer ratio in the first strain, DPF2G[pRKEH], while the carotenoid composition is not influenced by the levels of aeration [61]. However the second mutant strain, DPF2G[pRKEHX Δ 12], harbours a twelve-residue N-terminal truncation of PufX, giving core monomers that still have PufX [155]. These monomers represent one half of the RC-LH1-PufX core dimer, the structure of which was reported in [63, 64]. Biochemical data and atomic force microscopy data showed that the N-terminal truncation of PufX prevents dimerization of the core monomers [155-157], with 1 PufX and an estimated 15 LH1 subunits per monomer. These two mutants were grown so they had either high or low LH2 levels, and for simplicity these chromatophore samples will be referred to as dimeric low LH2 (DL) and dimeric high LH2 (DH), and monomeric low LH2 (ML) and monomeric high LH2 (MH), according to their core structure (monomeric or dimeric) and the high or low levels of LH2 present.

The DD13 double deletion strain of *Rba. sphaeroides* [70] for paper III was complemented with the desired genes to produce photosystems containing only the RC, only the LH1 or only the monomeric closed-ring RC-LH1 complexes devoid of PufX. All these materials contain spheroidenone as the main carotenoid. The RC-LH1-PufX complexes were extracted and purified from the WT *Rba. sphaeroides* strain 2.4.1 that has been genetically manipulated by deleting the neurosporene hydroxylase gene (CrtC) of the native carotenoid biosynthetic pathway. This strain develops core complexes mainly in dimeric RC-LH1-PufX form, irrespective whether the cells were grown photosyntheti-

cally or semiaerobically [61], and expresses a green carotenoid neurosporene rather than pheroidene/spheroidenone due to the complete deletion of the CrtC gene. The membrane samples with RC-LH1-PufX used here were also from this strain.

3.2. Sample Preparation for Optical Studies

All the samples were stored in freezer at -78°C until used. The defrosted concentrated samples were diluted before the experiments with the buffer solutions to obtain an optical density ≤ 0.1 in the cuvette to avoid emission reabsorption effects. The more concentrated samples (optical density up to 0.3) were used in fluorescence lifetime measurements to provide a greater signal, as necessary. To mimic the fluorescence decay times typical of the active RC condition, the membranes were mixed with 5 mM sodium ascorbate and 25 μM phenazinemethosulfate (PMS) along with the buffer solution. In case of the RC preparations, these chemicals were mandatory in every measurement to keep the RCs without being photo oxidized.

The sample solutions were placed in different holding cells depending on the specific need of the experiments. Most of the emission spectra were measured by placing the sample in a quartz cuvette. An additional homebuilt rotating cell of diameter 5 cm was used as a sample container along with quartz cuvette in intensity dependent fluorescence yield measurement (sections 4.1 and 4.2). The thickness of both sample holders was 2mm. The use of the two different kinds of sample cells, a stationary quartz cuvette and a rotating cell, enabled to cover the several orders of magnitude excitation intensity span from active (all RCs open) to saturated (all RCs closed) photosynthesis at reasonable signal to noise ratio. This is because like stirring, the rotating cell brings constantly into the excitable volume fresh portions of the sample with open RCs. Thereby, by reducing the saturation conditions for active photosynthesis are effectively achieved at higher average excitation intensity.

Increasing the excitation intensity beyond the saturated level results two or more excited states simultaneously available either in the same protein complex or in accessible radius for energy transfer. Double excitation of excitons leads to exciton annihilation due to ultrafast non-radiative relaxation of the doubly-excited states and both the fluorescence yield and lifetime of excitons will drop. This kind of quenching observed previously in WT membranes of *Rba. sphaeroides* under high repetition rate picosecond pulse excitation was assigned to annihilation between the singlet and triplet excitons [139, 158-161]. In this thesis we deliberately avoided exciton quenching by using the excitation intensities below the onset of non-linear excitation quenching range.

Most measurements in this thesis were performed at ambient (physiological) temperatures, 295 ± 3 K. However, the spectrally dispersive effects distinguishing the assembly of photosynthetic membranes described in section 4.3 can only be observed at cryogenic temperatures. To control the sample temper-

ature in these measurements, either a liquid nitrogen cryostat (Optistat DN, Oxford Instruments) or a liquid helium cryostat (Utreks) was used. The temperature was controlled with the precision of ± 0.5 K. In the low temperature measurements either gelatine capsules of 4 mm diameter or plastic (polymethyl methacrylate) cuvettes of 10 mm path length were used as sample container and glycerol was added to the buffer with a 2:1 volume ratio to secured transparent glassy samples. One has to be aware that co-solvents such as glycerol tend to coagulate purified proteins. This frequently manifests itself in steady state fluorescence measurements of the complexes as a red shift of the spectrum and in time-resolved fluorescence measurements as dispersive decay kinetics with shorter lifetime showing up at the blue side of the spectrum. Increasing the detergent (LDAO) concentration to $\sim 1\%$ usually prevents these artefacts when working with purified LH2 or LH1 complexes from *Rba. sphaeroides*.

3.3. Spectroscopy

For general characterization of the samples that has been studied in this thesis, a steady state absorption spectrometer (Model V-530, JASCO Corporation) was used. The absorption spectra of the samples in buffer solution were measured with a spectral resolution of 0.5 nm.

3.3.1. Steady-State Fluorescence Spectroscopy

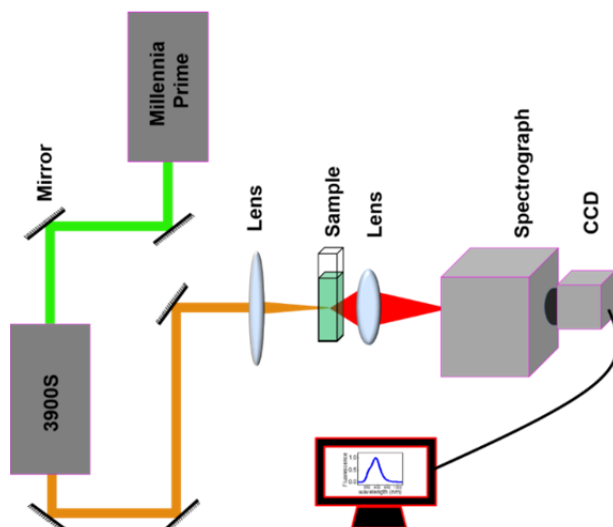


Fig. 3.1. The steady-state fluorescence spectrometer set-up, see text for details.

A schematic diagram of the steady-state fluorescence spectrometer is presented in Fig. 3.1. It consists of a narrow band (0.03 nm) continuous wave Ti:sapphire laser with tuning range of 675–1000 nm (3900S, Spectra Physics) pumped by a Millennia Prime diode pumped solid state laser (Spectra Physics) and a spectrograph (Shamrock 303i, Andor Technology) coupled with a CCD camera (DV420A-OE, Andor Technology). In intensity dependent fluorescence yield measurement, the maximum output power of the excitation laser was successively attenuated by an appropriate combination of neutral density filters. The fluorescence was collected at 90° with respect to the direction of excitation beam. The spectral resolution of the recorded signal was of 0.3 nm. The laser beam spot varied between 0.45–2 mm depending on the experiments.

3.3.2. Picosecond Time-resolved Fluorescence Spectroscopy

The general set-up of the time-resolved fluorescence spectrometer is schematically similar to the steady-state spectrometer, except that in the time-resolved version (i) the excitation light source is a pulsed laser, (ii) the spectrometer is either a subtractive-dispersion monochromator or a suitable set of band-pass filters, and (iii) photons are recorded by either a streak camera system in the synchroscan mode or a photomultiplier/avalanche photodiode in the time correlated single photon counting (TCSPC) system. Both of these recording systems are detailed in the following section. Irrespective of the recording technique, the samples were excited either using a continuous wave mode-locked Ti:sapphire laser (Coherent Mira-900) with the tuning range of 690–1000 nm, pulse repetition rate of 76 MHz, and pulse duration of ~ 100 fs (corresponding to an excitation spectral bandwidth of ~ 15 nm) or using a continuous wave picosecond dye laser (Coherent 700, tuning range 570–880 nm, 76 MHz, 2–3 ps, ~ 5 nm). In intensity dependent measurements the fluorescence was sent to the recording system through a specially selected band-pass filter (F42-900 Emitter HQ 900/50, AHF Analysentechnik). In spectrally dependent kinetic measurements, the fluorescence was recorded through a double subtractive-dispersion monochromator (DTMc300, Bentham Ltd.). In different time-resolved measurements, the recording spectral window varied between 2 to 5 nm.

The simplified schematic of a synchroscan streak camera based picosecond fluorescence spectrometer is presented in Fig. 3.2. This scheme emphasise the operation of the streak camera as follows. The fluorescence excited by the high repetition rate laser source directed to the photocathode of the streak camera. The photocathode converts the incident light photons into electrons proportional to the incident light intensity. The electrons are accelerated through a pair of accelerating electrodes and enter the deflecting field between a pair of deflecting plates. A high-amplitude (~ 3 kV peak to peak) sinewave voltage, synchronized with the excitation source, is applied to the deflection plates to sweep the electron depending on the phase of the deflecting voltage. The shorter electron bunch resulting from shorter light pulse feel the sweeping field for a

short time, and correspondingly, gets spatially deflected only a little bit. The longer pulses on the other hand get proportionally more deflected. This way the vertical spatial coordinate is transformed into a time axis. The swept electron image projected into the micro-channel plate (MCP) amplifier is electronically intensified to get a crisp luminescence image in a phosphor screen. The unchanged signal intensity along the horizontal spatial coordinate is just summed up/averaged by the CCD camera electronics and the digitalized read-out signal is directed into a computer for analyses.

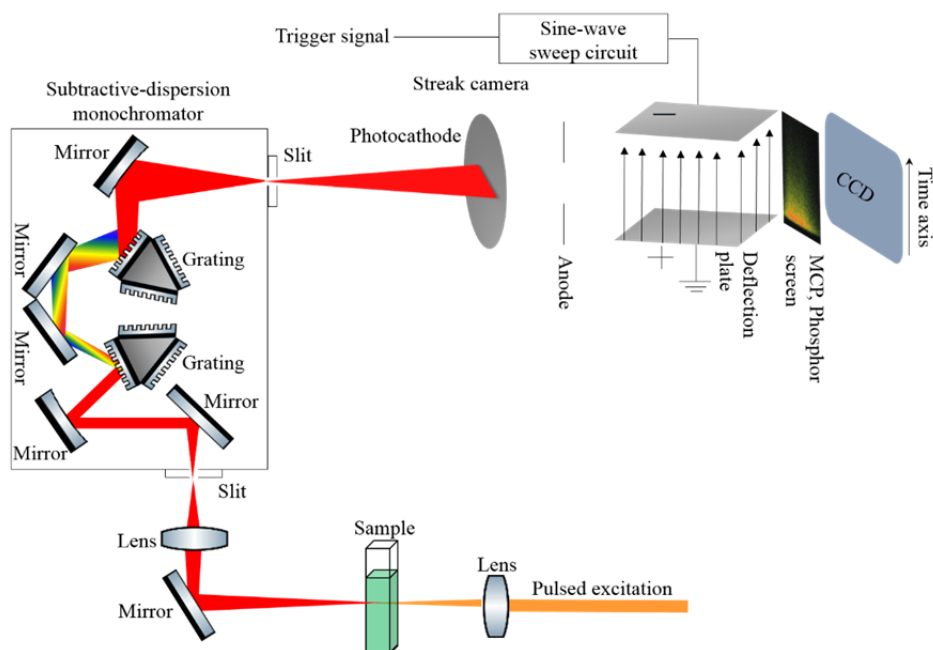


Fig. 3.2. The synchroscan streak camera based picosecond fluorescence spectrometer. Two versions of picosecond time-resolved streak camera set-ups, one home-built [162] and another commercially available (C1587, Hamamatsu) system were employed to obtain the time-resolved fluorescence data presented in this thesis. The temporal resolution, determined as the full width at the half maximum of the instrument response function, in the current experiments was 10 ps and 20 ps, respectively, in C1587 and in home-built streak camera system.

The high repetition rate operation of the streak camera is known as the synchroscan mode operation. The main advantage of this technique is that very faint emissions can be measured with high (order of 1 ps) time resolution, achieved by precise synchronization of the high repetition rate excitation laser pulses and the detection system. In the context of this thesis, this means that rather low-energy excitation pulses can be applied, perfectly safe for the protein materials studied. A downside of this technique, at least in current implementation, is relatively low achievable signal to noise ratio.

The TCSPC technique is an excellent replacement for longer (tens of picoseconds to nanoseconds duration) fluorescence lifetime measurements, as it provides a better signal-to-noise ratios than the streak camera. The principle of a classical TCSPC is the detection of single photons and the measurement of their arrival times in respect to a reference signal, usually the light source. TCSPC is a statistical method requiring a high repetitive light source to accumulate a sufficient number of photon events for a required statistical data precision. TCSPC electronics can be compared to a fast stopwatch with two inputs. The clock is started by the START signal pulse (usually the pulse from the excitation source) and stopped by the STOP signal pulse corresponding to detection of a photon. The time measured for one START – STOP sequence will be represented by an increase of a memory value in a histogram, in which the channels on the x-axis represent time. With a high repetition rate light source millions of START – STOP sequences can be measured in a short time. The resulting histogram counts versus channels will represent the fluorescence intensity versus time. In this classical configuration of TCSPC, since the single photon condition should be met, there are many pulse periods in which no photon is detected. In these periods the time-to-amplitude converter (TAC, see Fig. 3.3) is started but not stopped. As a result there must be a circuit in the TAC that detects the out-of-range condition, and resets the TAC for the next signal period. The frequent START-only events and subsequent resets are no problem at low pulse repetition rates. However, application of the classical START – STOP scheme in case of high pulse repetition rate light source (like the 76 MHz Coherent Mira-900) is impractical and should be replaced by the reversed START – STOP configuration [163, 164]. In the reversed START – STOP configuration, the START signal is derived from the photon event and the STOP signal is delivered by the pulse from the excitation source. Therefore, the TAC has to work only at the rate of photon detection event, not at much higher rate of the excitation pulses.

The TCSPC fluorescence spectrometer used in this study is presented in Fig. 3.3. The fluorescence followed by an excitation pulse from the sample is recorded by a detector and analysed by the device highlighted with the dotted line box. The pulse delivered by the detector as well as the reference (synchronisation) light signal is processed by a constant fraction discriminator (CFD) which avoids a pulse-height induced timing jitter. The output pulses of the CFDs are used to START (when a photon is detected) or STOP (with next reference pulse) the TAC circuit. The TAC uses a current source to switch on and off a capacitor in relation to the START and STOP pulse respectively, and generates an output signal proportional to the time between the START and the STOP pulses. The TAC signal is then fed to the analog-to-digital converter (ADC) and further processed by a multi-channel analyzer (MCA) to produce the final data output.

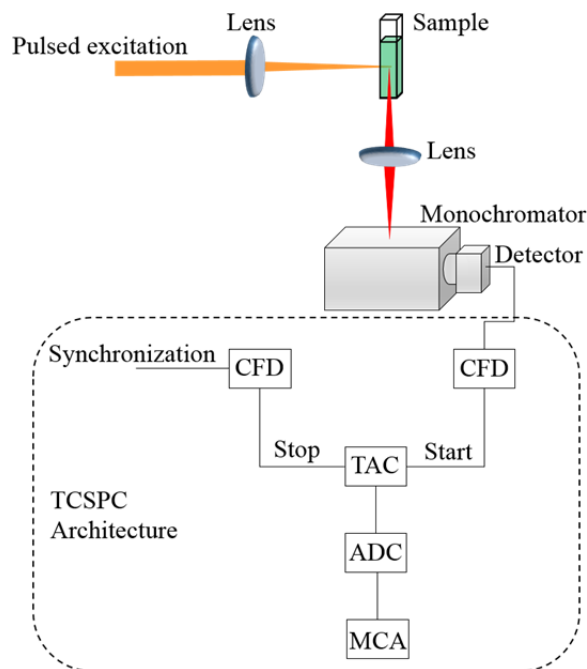


Fig. 3.3. The TCSPC picosecond time-resolved fluorescence spectrometer set-up. A commercially available TCSPC (SPC-150, Becker& Hickl GmbH) system was utilized to measure the longer fluorescence lifetime with high signal to noise ratio. Two different fluorescence detectors were used along with the TCSPC system: a hybrid photomultiplier detector (HPM-100-50, Becker& Hickl GmbH) with ~ 140 ps instrument response function and an avalanche photodiode (ID 100-50, ID Quantique) with ~ 70 ps instrument response function.

3.4. Data Analysis

The absorption spectra were corrected by subtracting the reference spectrum that was measured using the buffer solution in similar condition as the sample measured. In order to remove the residual light scattering, which primarily affects the spectra of chromatophores at $\lambda < 550$ nm, a mild correction was additionally applied by multiplying the measured spectra by λ^{-3} . The stationary fluorescence spectra were corrected for the spectral sensitivity of the set-up.

Two different data analysis methods were applied to obtain the lifetimes from the experimentally measured time-resolved fluorescence signal, viz single decay and global decay analysis. The global analysis is nothing but the single-decay fitting performed simultaneously at all detection wavelengths. The main advantage of employing global analysis is that it allows extracting from the data set only the information consistently evident at all detected wavelengths, reducing possible number of parameters. The two analysis methods were used here for consistency test of each other.

A major part of the time-resolved fluorescence experiment in this study has been performed using single decay analysis. The fluorescence kinetic signal, $S(t)$, recorded at certain detection wavelength, λ , can be approximated mathematically as follows:

$$S(t, \lambda) = \sum_i^n A_i(\lambda) \times e^{-\frac{t}{\tau_i}}, \quad (3.1)$$

where A_i and τ_i are the amplitudes and decay times of individual decay components. Every measured decay kinetics trace was fitted separately using the Spectra Solve (Version 2.0, LASTEK Pty. Ltd) software with an experimental instrument response function. The kinetic traces were appropriately corrected to the spectral and spatial sensitivity of the instrument in prior to the analysis. Most of the observed decays were double-exponential. For those the weighted lifetime was evaluated as follows:

$$\tau_{av} = \frac{A_1\tau_1 + A_2\tau_2}{A_1 + A_2}, \quad (3.2)$$

where A_1 , A_2 , τ_1 , and τ_2 are the amplitudes and decay times of individual decay components.

Global analysis was performed using open-source software Glotaran. In Glotaran, there is three way of analysing the spectrally dependent lifetime data. These are parallel decay fitting, sequential decay fitting and target analysis (a compartmental model). The target analysis provides the relative intensity contribution of each decay component as well as the relative intensity contribution from individual species as a function of wavelength, respectively known as decay associated spectra (DAS) and species associated spectra (SAS). All the lifetimes determined in this work have an experimental uncertainty from 5 to 10% of the obtained lifetime values, depending on the signal to noise ratio.

4. RESULTS

4.1. Efficiency of Light Harvesting in *Rhodobacter sphaeroides* Adapted to Different Levels of Light (Paper I)

This thesis was started by addressing the following fundamental question – how does the addition of peripheral antenna influence the rate of delivery of excitation energy to the RCs and the quantum efficiency of charge separation? This is not a new problem. A numbers of such studies can be found in the literature, see for example [165] and references therein. However, little quantitative data are available. In the present work, we have studied the excitation intensity dependent spectral and kinetic fluorescence responses of the chromatophore membranes from *Rba. sphaeroides* grown under carefully controlled lighting conditions. A special kinetic model was worked out and applied for analysis of the experimental data, as described in sections 1.4.3 and 1.4.4. The analysis yielded the microscopic rate constants that characterize the energy transfer and trapping efficiency in PSU on the ratio of the peripheral LH2 and core LH1 antenna complexes as well as on the wavelength of the excitation light.

The above Fig. 1.5 provides a sense how the absorption spectrum in the near-infrared spectral range changes in dependence whether the samples have been prepared under high ($1500 \mu\text{E}/\text{m}^2/\text{s}$) and low ($100 \mu\text{E}/\text{m}^2/\text{s}$) actinic irradiation, respectively. The detailed procedure to quantitatively evaluate the ratio of distal and core antenna complexes (LH2 to LH1 ratio or LH2/LH1 for short) is explained in section 1.2.2 (also in [105]).

Figure 4.1 and Table 4.1 outline the spectrally integrated (875–925 nm, see section 3.2) fluorescence lifetime in the WT membrane samples with different LH2/LH1 ratio and in core-only complex (at LH2/LH1=0). The fluorescence quenching time increases as the LH2/LH1 ratio increases irrespective of the state of the RC, i.e. either open (active) or closed (saturated). It also appears that despite the systematic increase of the lifetimes corresponding to closed and open state, their ratio is within the experimental uncertainty constant and close to 3.

These observations can be justified as follows. The peripheral antenna network found in LL adapted membranes is more extended in comparison with HL adapted membranes. Under low excitation light intensity almost all RCs are active, the explored membrane region before trapping is minimal, and correspondingly, average exciton lifetime is short. At high excitation intensity most of the RCs are closed, allowing larger portions of the membrane to be explored before trapping which increases the average lifetime of excitons. The RC-LH1-PufX-only membrane has no distal antenna [63, 69] resulting in the shortest possible fluorescence lifetimes. The fact that the saturated state lifetime in RC-LH1-PufX-only membranes appears significantly shorter than in LH1-only membranes speaks for quenching of excitons by closed RCs, as explained in [63, 69].

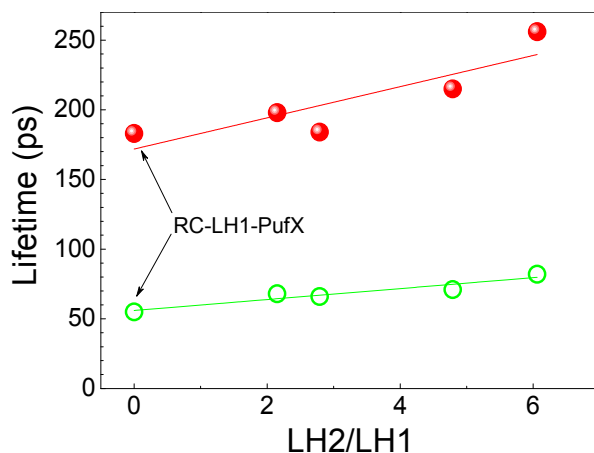


Fig. 4.1. The spectrally integrated fluorescence decay time corresponding to active (green open circles) and saturated (red spheres) phases of photosynthesis as a function of LH2 to LH1 ratio. The arrows indicate lifetimes in tubular membranes comprising sole dimeric core complexes. The fluorescence was excited at 590 nm. The lines represent linear fits of the data points.

Table 4.1. Fluorescence lifetimes corresponding to active and saturated ranges of photosynthesis.

Sample (LH2/LH1)	τ_{av} (ps)		$\tau_{av}(\text{closed})/\tau_{av}(\text{open})$
	Active	Saturated	
RC-LH1-PufX (0)	55 ± 2	183 ± 5	3.3 ± 0.4
HL116 (2.15)	68 ± 2	198 ± 4	2.9 ± 0.4
HL133 (2.79)	66 ± 2	184 ± 7	2.8 ± 0.4
LL181 (4.79)	71 ± 2	215 ± 5	3.0 ± 0.4
LL196 (6.06)	82 ± 3	256 ± 7	3.1 ± 0.4

High quantum efficiency of trapping over 80% was observed in most cases, which decreased toward shorter excitation wavelengths within the near infrared absorption band, as can be seen in Fig. 4.2. The maximum calculated efficiency of $\eta = 88.1\%$ was found in case of the core-only complexes, by assuming there were no losses in exciton transfer. The general behaviour in the chromatophore efficiency is that decreases with increasing the peripheral antenna size, i.e. increasing LH2/LH1 ratio. Although the drop of efficiency upon 915 nm excitation on LH2/LH1 ratio is small, only $\sim 1\text{--}2\%$, it is significantly enhanced at 800-nm excitation. The reduced efficiency in the latter case is conceivable because the exciton now probes the longer LH2- \rightarrow LH1- \rightarrow RC pathway involving

LH2, compared to only LH1->RC transfer with 915 nm excitation. This indicates that any difference in the calculated efficiency in monomeric and dimeric chromatophores excited at 800 nm and 915 nm, notifies us about the LH2->LH1 transfer. The decline in efficiency upon 800 nm excitation on LH2/LH1 perfectly follows the LH2 to LH1 transfer rate, k_1 , see section 1.4.3. The calculated efficiency further decreases if there is any disconnected or poorly connected LH2 units present in the sample.

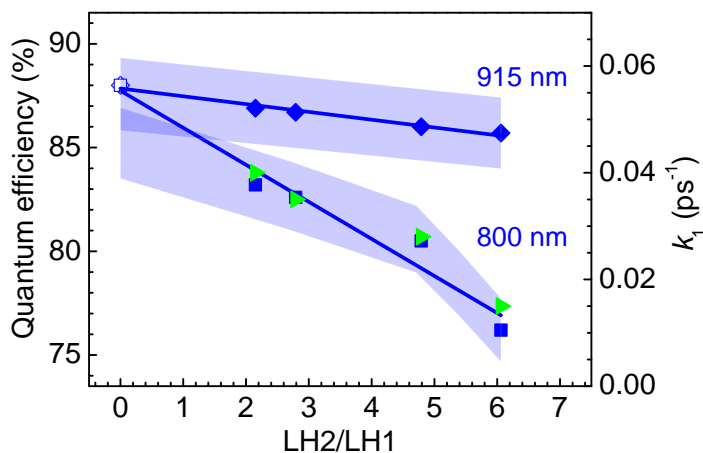


Fig. 4.2. The calculated quantum efficiency of active photosynthesis relative to the LH2 to LH1 protein ratio upon excitation at 800 nm (squares) and at 915 nm (rhombi). The efficiency of sole core complexes (RC-LH1-PufX) is designated by the open data point at LH2/LH1=0. The green triangles and right hand scale relate to the forward energy transfer rate, k_1 . The lines represent the linear fits of the data points. The estimated standard deviation of about 2% in calculated efficiency is highlighted by the shaded area.

4.2. Dimerization of Core Complexes as an Efficient Strategy for Energy Trapping (Paper II)

In *Rba. sphaeroides*, light harvesting LH2 complexes transfer the absorbed solar energy to RC-LH1-PufX core complexes, which are mainly found in the dimeric state. Many other purple phototrophs have monomeric core complexes and the basis for requiring dimeric cores is not fully established. Therefore, we set to analyse mutant strains of *Rba. sphaeroides* that contain either native dimeric core complexes or altered monomeric cores harbouring a deletion of the first 12 residues from the N-terminus of PufX. This retains the PufX polypeptide but removes the major determinant of core complex dimerization. The chromatophore membranes for our experiments were purified from strains with dimeric or monomeric cores, and with either high or low levels of the LH2 complex. The samples were interrogated with picosecond time-resolved fluo-

rescence kinetic spectroscopy at varying excitation intensity and wavelength to reveal their light-harvesting and energy trapping properties. A graphical summary of the experiments presented in this section is shown in Fig. 4.3.

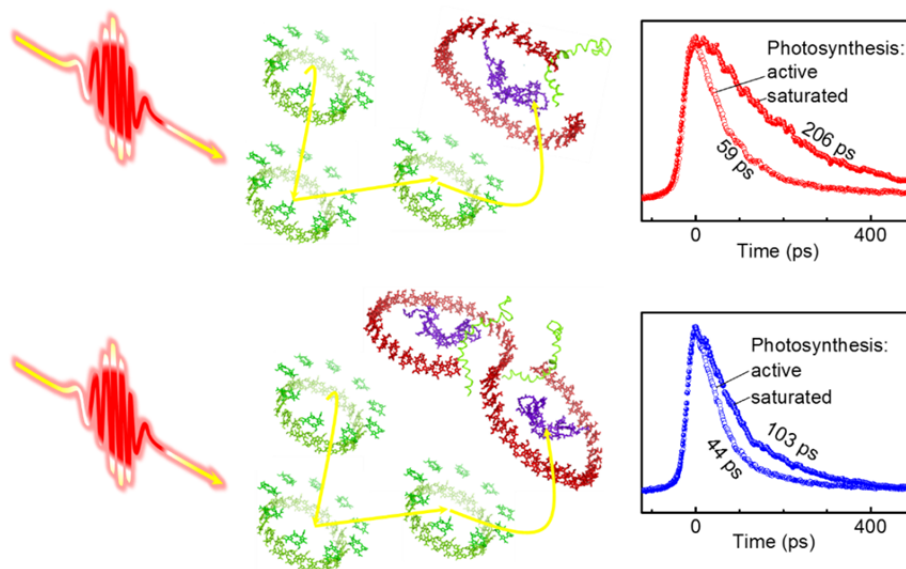


Fig. 4.3. Graphical summary of the experiments presented in section 4.2.

The excitation light intensity dependence of the fluorescence yield and lifetime in monomeric and dimeric core samples are presented in Fig. 4.4. This result shows a generic increase of the fluorescence yield and lifetime with the excitation light intensity. It is noticeable that the fluorescence lifetimes from the samples containing monomeric cores (ML and MH) have almost twice higher values than those from the samples with dimeric cores (DL and DH) at all excitation intensities. Compared to that great difference, the difference in fluorescence lifetimes between the samples having different LH2 content but similar core structures (MH vs. ML or DH vs. DL), as discussed in paper I, appears relatively insignificant.

The physical reason behind the dissimilarity in exciton trapping time between these core complex organizations is not quite clear. However the shorter lifetime for dimeric complexes can be suggested due to excitation sharing across a larger LH1 antenna with access to two traps, i.e. the presence of two RCs instead of one per LH1 assembly, resulting in increased trapping or quenching probability of LH1 excitons at low or high excitation intensity, respectively. Another effect that can vary the lifetime may arise from core monomers reorganising the photosynthetic membrane, as shown in the atomic force microscopy topographs recorded in a previous study [156]. Comayras et al

[166] previously showed that such excitation sharing occurs; the current study explains how this may improve the photosynthesis efficiency.

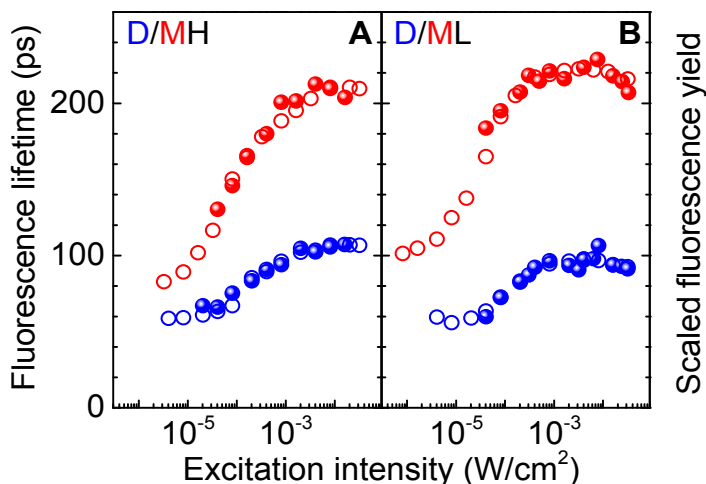


Fig. 4.4. Excitation intensity dependence of the fluorescence yield (open circles, right Y-axis) and the dominant short fluorescence lifetime component (filled spheres, left Y-axis) in the dimeric (blue) and monomeric (red) core samples. The data of high and low LH2 content samples respectively presented in panel A and B. In order to visualize the proportionality between the yield and the lifetime, the yield data are scaled until matching with lifetime values. In kinetic measurements the fluorescence was excited at 590 nm while in stationary fluorescence yield measurements it was at 800 nm.

Figure 4.5 shows the calculated quantum efficiency in the dimeric and monomeric core samples. It is evident that the quantum efficiency is consistently found higher in the samples with dimeric core. Like established in paper I, the efficiency drops as the LH2/RC ratio increases and the absolute efficiency is always higher at 915-nm excitation compared with 800-nm excitation irrespective of the structure of the core complex. Alternatively, the quantum efficiency of the sole core complex should be the same, irrespective of the excitation wavelength. Indeed within the experimental uncertainty, the linear fits of the data points in Fig. 4.5 converge at LH2/RC = 0. The relatively poorer convergence in case of monomeric core samples most probably results from functionally disconnected or poorly connected LH2 units in these samples. Such units can be traced back by long lifetime components of the fluorescence decay kinetics, being observed to be relatively more significant in the kinetics of the monomeric-core samples than in the dimeric-core ones.

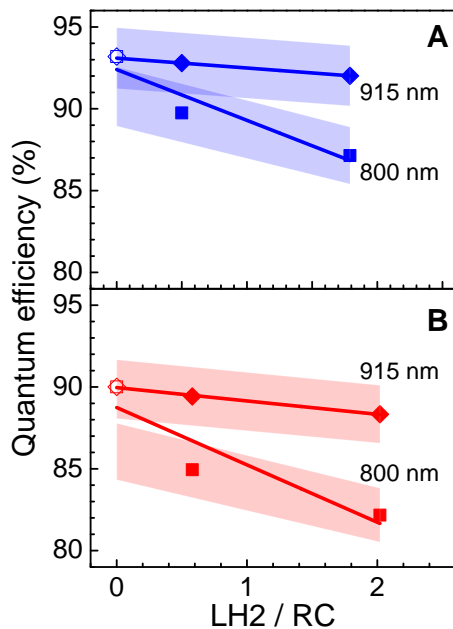


Fig. 4.5. The calculated quantum efficiency of active photosynthesis relative to the LH2 to RC ratio in dimeric (A) and monomeric (B) core samples upon 800 (squares) and 915 nm (rhombi) excitation. The unfilled data points at LH2/RC=0 represent the quantum efficiencies of the model membranes containing either only dimeric or only monomeric core complexes. The coloured area displays the ~2% estimated standard deviation in the efficiency. The lines show linear fits of the data points.

4.3. Spectral and Kinetic Effects Accompanying the Assembly of Core Complexes (Paper III)

One of the prime motivations for this work was that the many literature data on the excitation energy transfer and trapping in photosynthetic bacterial membranes appear fragmented, irregular, and sometimes even controversial. This unsatisfactory situation is frequently vaguely assigned to “biological variability”. To make order in at least some of these data, we systematically studied a range of core complexes from one and the same species of *Rba. sphaeroides*, using similar, carefully selected and controlled experimental conditions over the broad temperature range of 4.5–300 K. Secondly, we wanted to see whether the increased energy trapping efficient found in the specific mutant chromatophore membranes consisting dimeric core complexes persists in the case of the membranes comprising sole core complexes.

To set the stage, Fig. 4.6 reviews the spectrally dispersive emission kinetics at cryogenic temperatures on the core complexes that devoid of RC both in isolated or membrane embedded state. It is evident that in sole LH1 complexes the fluorescence kinetics is radically different, depending on whether the complexes

are organized into the functional membrane network or isolated into the detergent micelles. The fluorescence lifetime recorded in case isolated LH1 complex shows a moderately long fluorescence lifetime of ~ 1.4 ns at the blue edge of the emission spectrum that gradually shortens toward longer wavelengths. Past about 895 nm the lifetime stabilizes at the level of ~ 1 ns. In contrast, in the membrane embedded sample the lifetime at the blue edge of the emission spectrum greatly shortens, being limited by the temporal resolution of our set up. The lifetime gradually elongates toward longer wavelengths until past ~ 915 nm it stabilizes at the same level (~ 1 ns) as in the isolated LH1 complex.

The data in Fig. 4.6 corroborate the records for peripheral LH2 proteins [141, 167-169]. In these earlier works the distinctive longer lifetime observed at the short-wavelength in case of isolated complexes was assigned to fundamental properties of exciton polarons in an energetically heterogeneous ensemble of individual complexes [170]. In an energetically connected membrane networks due to the possible excitation energy transfer and funnelling towards energetically lowest complexes, the lifetime distribution characteristic for individual complexes turns out to be completely hidden [171-173].

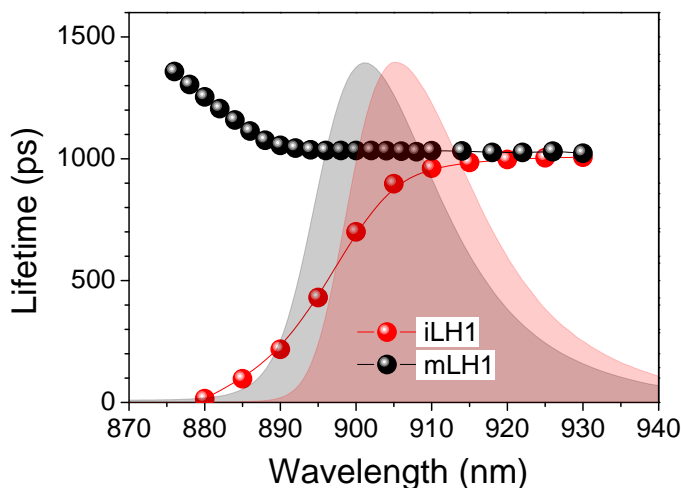


Fig. 4.6. Dependence of the fluorescence lifetime on the recording wavelength in isolated and membrane LH1 complexes measured at 5 K. The data for isolated and native membrane-embedded LH1 complexes are distinguished by black and red, respectively. Reference fluorescence spectra of the samples using similar colour codes are shown in the background. The fluorescence was excited at 860 nm and recorded with spectral resolution of 2 nm. The lines connecting data points are for leading the eye only.

Figure 4.7 confirms that the dispersive fluorescence kinetics observed in the core membranes lacking RCs is also qualitatively followed in the core membranes that include RCs. Yet quantitative numbers are rather different. This is most clearly seen when the limiting long-wavelength (past 915 nm) lifetimes

are compared. In the RC-less mLH1 sample this lifetime is ~ 1 ns, while in the membrane-embedded core complexes complete with RCs it is 300–400 ps, more than twice shorter. This significant shortening of the fluorescence lifetime is no doubt caused due to added quenching of antenna excitons by the RCs, either in closed or open state as described in Introduction. Even more noteworthy is that the fluorescence in the monomeric system decays consistently slower than in the dimeric system, validating the data of paper II at cryogenic temperatures.

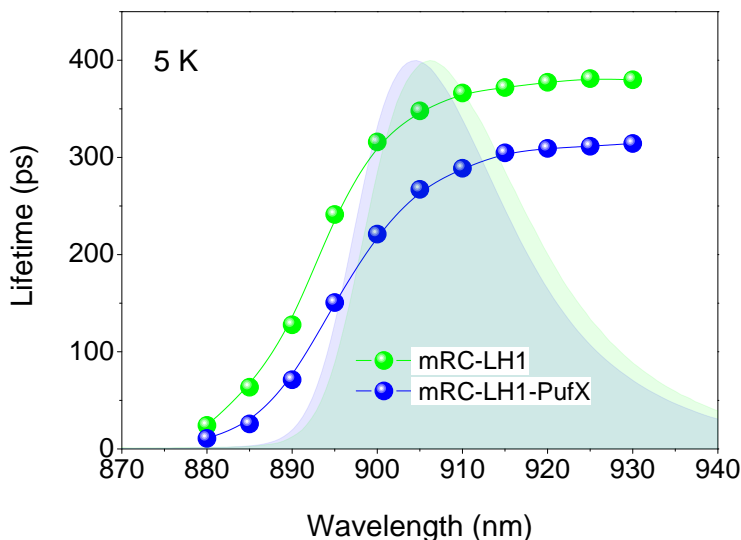


Fig. 4.7. Fluorescence lifetime as a function of recording wavelength at 5 K for the membrane-embedded monomeric (green) and dimeric (blue) core complexes in the presence of RC. The fluorescence was excited at 860 nm and recorded with spectral resolution of 4 nm. Saturating excitation intensity was used corresponding to closed RC state (most RCs photo-oxidized). The reference fluorescence spectra in the background are drawn with matching colours.

Temperature dependence of the fluorescence decay time is presented in Fig 4.8. In isolated complexes, irrespective the presence of RC, the decay time stays constant up to relatively high temperatures. In membrane samples, in contrast, thermal quenching of the lifetime sets in already at very low temperatures and the drop continues all the way up to ambient temperatures, where the lifetime value reaches about half of its value at 5 K. Similar thermal behaviour was previously observed in membranes of LH2 complexes [141, 167-169] and explained within the already introduced paradigm of inter-connected network of protein complexes, where the occasional quenchers localized in separate membrane areas become increasingly available for quenching with the raising temperature. It is also evident from Fig. 4.8 that in the same broad temperature

range the fluorescence lifetime in monomeric (mRC-LH1) core complexes is longer than in dimeric (mRC-LH1-PufX) core complexes. One thus might conclude that at all temperatures the solar excitation energy harvesting by dimeric core complexes is more efficient than it is by monomeric complexes.

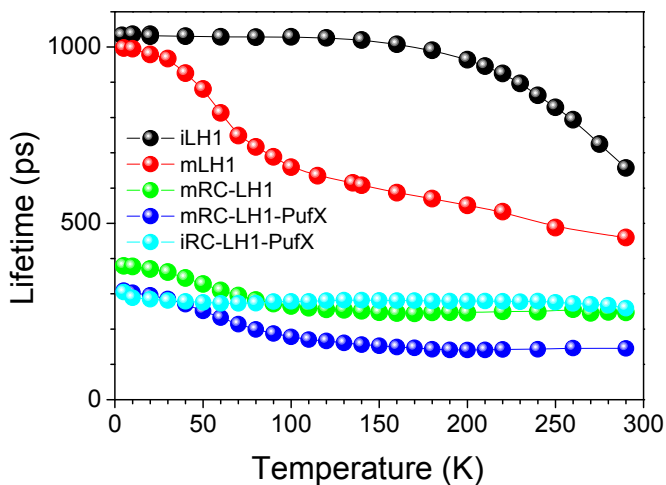


Fig. 4.8. Temperature dependence of the fluorescence decay time in various indicated core complexes. The fluorescence was recorded at red side of the fluorescence spectrum (at 920 nm between 5 and 230 K and at 890 nm above 230 K) following the excitation at 860 nm with spectral resolution of 4 nm.

5. SUMMARY AND FURTHER CHALLENGES

Recent studies by scanning tunnelling microscopy on the intracytoplasmic membrane of purple anoxygenic photosynthetic bacteria at sub-nanometer resolution provided remarkable images showing the nano-scale structural adaptation of photosynthetic membranes in response to their changing habitats. This thesis deals with the effects of such nano-scale structural arrangements of the photosynthetic membrane on the delivery rate of photo-excitations into the RC traps and on the quantum efficiency of charge separation at the RCs. In order to gain information about such connections, the photosynthetic membranes extracted from native and genetically mutated species of *Rba. sphaeroides* were interrogated with a combination of optical absorption, steady-state and time-resolved fluorescence spectroscopy. The major outcomes of this research are summarized below.

1. From the perspective of the ecological habitat of the photosynthetic purple bacteria, the formation of a higher concentration of peripheral antenna is facilitated by growth under dim light even though the energy trapping is slower in low light adapted membranes. The similar values for the trapping efficiencies in all samples imply a robust photosynthetic apparatus that functions effectively at a variety of light intensities.
2. In the native membranes of the photosynthetic purple bacterium *Rba. sphaeroides*, the presence of PufX protein in the core complexes causes most of them to assemble into an S-shaped dimeric structure. Only a small percentage of core complexes have been found to form open-ring-shaped PufX-containing monomers. At the same time, in several other purple bacteria the closed- or open-ring-shaped monomeric core complexes dominate. The reason for this structural disparity is unknown. We discovered by experimenting with specially designed species of *Rba. sphaeroides* that the energy trapping time in the mutant chromatophore membranes containing mostly monomeric core complexes along with LH2 complexes is significantly longer compared with that in the membranes with dimeric cores and LH2s. This result was confirmed on the mutant membranes that contained just monomeric or dimeric core complexes. We conclude that at least in *Rba. sphaeroides* species the energy trapping is more efficient when the photosynthetic membranes incorporate dimeric-core complexes.
3. The multiple factors that influence mostly the fluorescence lifetime of the core complexes either in detergent-isolated or membrane-embedded form have been revealed, providing a more comprehensive understanding of the field. These factors include the presence or absence of RC, the supramolecular architecture (monomeric or dimeric) of the complexes and whether the complexes were studied in native membrane environment or in detergent- purified state.

One of the most unexpected results of this study is the observed elongated energy trapping time by the monomeric core complexes compared to that of the dimeric core complexes. This effect evades straightforward explanation if similar antenna exciton hopping time between LH1 and RC compartments holds in both types of core complexes. Future efforts are, therefore, in order by expanding towards well-characterized monomeric and dimeric core complexes from other species studied under well-defined experimental conditions. In full scale, however, this goal would require concerted advancement of biochemical, structural and theoretical methods.

SUMMARY IN ESTONIAN

Ergastusenergia pikosekundilise migratsiooni ja lõksustamise nanostruktuursed piirangud bakterite fotosünteesilistes membraanides

Mitteoksügeensete fotosünteesivate bakterite tsütoplasmasiseste membraanide hiljutised uuringud sub-nanomeetrilise eraldusvõimega skaneeriva tunnelmikroskoobiga on näidanud fotosünteesivate membraanide nanostruktuurset kohastumist erinevatele keskkonnatingimustele. Käesolev dissertatsioon käsitleb fotosünteesivate membraanide nanostruktuuride ümberkorralduste mõju esmastele fotosünteesilistele protsessidele: valgusergastuste ülekande kiirusele reaktsioonitsentrite suunas ja nende lõksustumise efektiivsusele. Nende seoste avastamiseks viidi läbi mõõtmised purpurbakterite *Rba.sphaeroides* looduslikest ja geneetiliselt muundatud tüvedest eraldatud membraanidega, kasutades nii optilise neeldumise kui ka statsionaarse ja aeglahutatud fluorestsentsi meetodeid. Dissertatsiooni põhilise tulemused on kokkuvõtvalt järgnevad.

1. Fotosünteesiliste purpurbakterite elukeskkonnas soodustab hämar valgus suuremat perifeersete antennide moodustumist, kuigi nõrgale valgusele kohanenud membraanides on valgusenergia lõksustumise kiirus langenud. Samas valgusenergia lõksustumise sarnased kasutegurid kõikide uurimise all olnud erinevatele elukeskkonna tingimustele kohanenud objektides viitavad laias valguse intensiivsuste vahemikus efektiivselt toimiva võimeka ja vastupidava fotosünteesilise aparatuuri olemasolule.
2. PufX valgu olemasolu loodusliku fotosünteesiva purpurbakteri *Rba.sphaeroides*'i membraanide LH1 tuumkompleksides põhjustab enamikul juhtudel nende komplekside S-kujulise dimeerse struktuuri moodustumist. Ainult väike osa PufX-sisaldavatest tuumkompleksidest moodustab avatud ringi kujulise monomeeri. Mitmetes teistes purpurbakterites domineerivad suletud või avatud ringi kujulised monomeersed tuumkompleksid. Sellise struktuurse erinevuse põhjus on teadmata. Uurides spetsiifiliselt modifitseeritud *Rba.sphaeroidese* objekte, avastasime, et energia lõksustumise aeg membraanides, mis koosnevad põhiliselt monomeersetest tuumkompleksidest ja LH2 kompleksidest, on tunduvalt pikem võrreldes dimeersete kompleksidest ja LH2'dest koosnevate membraanidega. See tulemus leidis kinnitust ka ainult monomeersetest või dimeersetest tuumkompleksidest koosnevate mutantsete membraanide korral. Siit järeldame, et vähemalt purpurbakteri *Rba.sphaeroides* korral on energia lõksustumine efektiivsem kui fotosünteesivates membraanides sisalduvad dimeersed tuumkompleksid.
3. Töös on välja selgitatud mitmed tuumkomplekside fluorestsentsi eluiga oluliselt mõjutavad tegurid nii detergendiga isoleeritud kui ka membraanisestest komplekside jaoks. See annab võimaluse antud uurimisvaldkonna paremaks mõistmiseks. Mõjuteguritena võib nimetada reaktsioonitsentrite olemasolu või puudumist tuumkompleksides, komplekside

supramolekulaarset arhitektuuri (monomeerne või dimeerne) ning kesk-
konda, milles komplekse uuriti (membraani integreeritud või detergen-
diga isoleeritud).

Selle töö kõige ootamatumaks tulemuseks on monomeerse struktuuriga tuum-
kompleksides jälgitud energia lõksustumise kiiruse oluline aeglustumine võrrel-
des lõksustumise kiirusega dimeerse struktuuriga tuumkompleksides. Seda
efekti on keeruline seletada, eeldades, et antenni ergastuse hüppe aeg tuum-
kompleksidelt reaktsioonitsentritesse kestab sama kaua mõlemat tüüpi tuum-
komplekside korral. Edasised püüdlused on seotud ka teistest bakteriliikidest
valmistatud hästi karakteriseeritud struktuuriga komplekside uurimise edasi-
arendamisele selgelt määratletud eksperimentaalsetes tingimustes. Siiski, sellise
ülesande realiseerimine täies mahus eeldab biokeemiliste, struktuursete ja teo-
reetiliste uurimismeetodite kooskõlastatud edasiarendamist.

ACKNOWLEDGEMENTS

Pursuing this PhD thesis has been truly changed my life in many ways and it would have never been accomplished without the continuous support that I received from numerous people.

First and foremost, I am deeply grateful for my supervisor, Prof. Arvi Freiberg for giving a chance to do my PhD in his laboratory. Thanks for giving me constant encouragement, support, advices, caring and directions that I needed during the course of this thesis. Thanks for showing me different ways to approach a research problem and the need to be persistent to accomplish a goal. After all I thank you for having faith on me and for the time that you always found for me in your busy schedule. I cannot even imagine a better advisor. I shall always be indebted to you. Thank you very much Arvi!

Many thanks to Dr. Kõu Timpmann for patiently teaching me almost all the experimental techniques which I needed to perform the measurements and for teaching the analysis of measured data. It was always motivational to me to experience the joy and the enthusiasm you have towards the experiments. Without your guidance and constant feedback this PhD would not have been achievable. Thank you very much Kõu!

Special Thanks to Dr. Liina Kangur for her countless support over the past four years. You helped me to feel comfortably in the laboratory in the early days. Thanks for helping me to learn the basics of bacterial photosynthesis from a biochemist's perspective. I appreciate your inputs during the high-pressure measurements. Apart from all these, you became a true friend of mine and I remember the discussions we had about almost every subject. Thank you very much Liina!

My thanks also go out to Dr. Erko Jalviste for the help on various theories related issues. Thanks for teaching me the global fitting software, Glotaran. Thanks for the every bit of guidance that you provided to fulfil this thesis. Finally being a nice friend of mine, I remember all the nice talks we had, including the non-scientific ones. Thank you very much Erko!

My other colleagues are also greatly acknowledged for their support. I thank Dr. Margus Rätsep for helping with stationary fluorescence measurements and for the nice discussions. Many thanks to Dr. Juha Matti Linnanto and Dr. Dheerendra Yadav for helping to produce the structures of the antenna complexes presented in this thesis and for the fruitful discussions.

I extend my gratitude to all the other members of the Biophysics laboratory including the past members, Prof. Jörg Pieper, Dr. Kristjan Leiger, Dr. Mihkel Pajusalu and Hain Salujärv for their help at different stages of the preparation of this thesis.

I am grateful to Prof. C. Neil Hunter, Dr. John A. Timney and Dr. Peter G. Adams from the University of Sheffield, for providing the samples and helpful contributions in Paper I and Paper II.

Special thanks to Anne Luik-Ristikivi for her help and assistance concerning the employment contract paper works, residence permit issues and finally for all

the legal advices. Furthermore, I enjoyed the visit to your home together with Liina and Erko.

I express my gratitude to Dr. Safakath Karuthedath, this entire research stay is initiated with your help. Thanks for your support that you have been providing for the last eight years. I remember the adventures that we had in different cities in Europe and back in homeland. Thanks for the countless scientific and non-scientific talks we had through Skype.

I am grateful to the faculty members of M.E.A.S.S College, Areacode, for supporting to overcome many difficulties in my life. Without their help this endeavour wouldn't have fulfilled.

I thank Dr. Ramesh Ekambaram for being a nice friend and I recall all the wonderful time we had in Tartu during last four years.

I gratefully acknowledge Dr. Girinath G. Pillai for his inputs in preparing my second paper. I also thankfully remember all the nice time we had in Tartu and the adventure trip we made to St. Petersburg!

I also thank Dr. Xining Li for being such an exceptionally reliable friend. I remember all the good and adventure times we had in Estonia and in Finland, especially the car accident we had during the trip to Pärnu!

I am deeply indebted to my family: Amma, Achan, without your unconditional love, support and sacrifices this thesis would never have been written. Chechi, Tattan, being your little brother, you guys were always my privilege and I always found tremendous joy in hanging out with you guys!

Last but not least, I would like to thank those not mentioned above, who stand by me.

REFERENCES

1. Van Neil, C.B., The bacterial Photosynthesis and their Importance for General Problem of Photosynthesis. *Adv. Enzymol.*, 1941. **1**: p. 263–328.
2. Priestley, J. and W. Hey, *Observations on Different Kinds of Air*. By Joseph Priestley, L.L. D. F. R. S. Philosophical Transactions, 1772. **62**: p. 147–264.
3. Clayton, R.K., W.R. Sistrom, and Editors., *The Photosynthetic Bacteria*. 1978: Plenum, New York, N. Y. 946.
4. Blankenship, R.E., J.M. Olson, and M. Miller, *Antenna complexes from green photosynthetic bacteria*, in *Anoxygenic Photosynthetic Bacteria*, R.E. Blankenship, M.T. Madigan, and C.E. Bauer, Editors. 1995, Kluwer Academic Publishers: Dordrecht. p. 399–435.
5. Barnes, C.R., *On the Food of Green Plants*. *Botanical Gazette*, 1893. **18**(11): p. 403–411.
6. Messinger, J., et al., *Principles of photosynthesis Fundamentals of Materials for Energy and Environmental Sustainability*. 2011: Cambridge University Press.
7. Hohmann-Marriott, M.F. and R.E. Blankenship, *Evolution of Photosynthesis*. *Annual Review of Plant Biology*, 2011. **62**(1): p. 515–548.
8. Blankenship, R.E., et al., Comparing Photosynthetic and Photovoltaic Efficiencies and Recognizing the Potential for Improvement. *Science*, 2011. **332**(6031): p. 805–809.
9. Frölicher, T.L. and F. Joos, Reversible and irreversible impacts of greenhouse gas emissions in multi-century projections with the NCAR global coupled carbon cycle-climate model. *Climate Dynamics*, 2010. **35**(7): p. 1439–1459.
10. Kooten, G.C.v., *Climate Change, Climate Science and Economics. Prospects for an Alternative Energy Future*. Vol. XXIII. 2013, Dordrecht: Springer.
11. Janssen, P.J.D., et al., *Photosynthesis at the forefront of a sustainable life*. *Frontiers in Chemistry*, 2014. **2**(36).
12. Shaheen, S.E., D.S. Ginley, and G.E. Jabbour, *Organic-Based Photovoltaics: Toward Low-Cost Power Generation*. *MRS Bulletin*, 2005. **30**(1): p. 10–19.
13. Hagberg, D.P., et al., *Molecular Engineering of Organic Sensitizers for Dye-Sensitized Solar Cell Applications*. *Journal of the American Chemical Society*, 2008. **130**(19): p. 6259–6266.
14. Barber, J. and P.D. Tran, *From natural to artificial photosynthesis*. *Journal of The Royal Society Interface*, 2013. **10**(81).
15. Green, M.A., et al., *Solar cell efficiency tables (Version 45)*. *Progress in Photovoltaics: Research and Applications*, 2015. **23**(1): p. 1–9.
16. Nguyen, K. and B.D. Bruce, Growing green electricity: Progress and strategies for use of Photosystem I for sustainable photovoltaic energy conversion. *Biochimica et Biophysica Acta (BBA) – Bioenergetics*, 2014. **1837**(9): p. 1553–1566.
17. Kargul, J., J.D. Janna Olmos, and T. Krupnik, *Structure and function of photosystem I and its application in biomimetic solar-to-fuel systems*. *Journal of Plant Physiology*, 2012. **169**(16): p. 1639–1653.
18. Lewis, N.S. and D.G. Nocera, *Powering the planet: Chemical challenges in solar energy utilization*. *Proceedings of the National Academy of Sciences*, 2006. **103**(43): p. 15729–15735.
19. Luo, J., et al., Water photolysis at 12.3% efficiency via perovskite photovoltaics and Earth-abundant catalysts. *Science*, 2014. **345**(6204): p. 1593–1596.

20. , G. and D. Shevela, *Adventures with Cyanobacteria: A Personal Perspective*. Frontiers in Plant Science, 2011. **2**(28).
21. Gest, H., History of concepts of the comparative biochemistry of oxygenic and anoxygenic photosyntheses. *Photosynth. Res.*, 1993. **35**(1): p. 87–96.
22. Wraight, C.A. Current attitudes in photosynthesis research. in *Photosynthesis*. 1982. Academic, New York, N.
23. Xiong, J., et al., *Molecular Evidence for the Early Evolution of Photosynthesis*. *Science*, 2000. **289**(5485): p. 1724–1730.
24. Şener, M., et al., Förster Energy Transfer Theory as Reflected in the Structures of Photosynthetic Light-Harvesting Systems. *ChemPhysChem*, 2011. **12**(3): p. 518–531.
25. Mirkovic, T., et al., Light Absorption and Energy Transfer in the Antenna Complexes of Photosynthetic Organisms. *Chemical Reviews*, 2016.
26. Niederman, R.A., Structure, Function and Formation of Bacterial Intracytoplasmic Membranes, in *Complex Intracellular Structures in Prokaryotes*, J.M. Shively, Editor. 2006, Springer Berlin Heidelberg: Berlin, Heidelberg. p. 193–227.
27. Gibson, K.D., Isolation and Characterisation of Chromatophores from *Rhodospseudomonas spheroides**. *Biochemistry*, 1965. **4**(10): p. 2042–2051.
28. Oelze, J. and G. Drews, *Membranes of photosynthetic bacteria*. *Biochim. Biophys. Acta*, 1972. **265**(2): p. 209–39.
29. Prince, R.C., et al., Asymmetry of an energy transducing membrane. The location of cytochrome c₂ in *Rhodospseudomonas spheroides* and *Rhodospseudomonas capsulata*. *Biochimica et Biophysica Acta (BBA) - Bioenergetics*, 1975. **387**(2): p. 212–227.
30. Scheuring, S., et al., *The architecture of Rhodobacter sphaeroides chromatophores*. *Biochimica et Biophysica Acta (BBA) - Bioenergetics*, 2014. **1837**(8): p. 1263–1270.
31. Sener, M., et al., Overall energy conversion efficiency of a photosynthetic vesicle. *eLife*, 2016. **5**: p. e09541.
32. Blankenship, R.E., *Molecular Mechanisms of Photosynthesis*. 2002: Blackwell Science, Oxford, United Kingdom.
33. Zuber, H. and R.J. Cogdell, *Structure and Organization of Purple Bacterial Antenna Complexes*, in *Anoxygenic Photosynthetic Bacteria*, R.E. Blankenship, M.T. Madigan, and C.E. Bauer, Editors. 1995, Springer Netherlands: Dordrecht. p. 315–348.
34. Cartron, M.L., et al., Integration of energy and electron transfer processes in the photosynthetic membrane of *Rhodobacter sphaeroides*. *Biochimica et Biophysica Acta (BBA) - Bioenergetics*, 2014. **1837**(10): p. 1769–1780.
35. Jackson, P.J., et al., Quantitative proteomic analysis of intracytoplasmic membrane development in *Rhodobacter sphaeroides*. *Molecular Microbiology*, 2012. **84**(6): p. 1062–1078.
36. Woronowicz, K. and R.A. Niederman, Proteomic Analysis of the Developing Intracytoplasmic Membrane in *Rhodobacter sphaeroides* During Adaptation to Low Light Intensity, in *Recent Advances in Phototrophic Prokaryotes*, P.C. Hallenbeck, Editor. 2010, Springer New York: New York, NY. p. 161–178.
37. Freiberg, A., *Coupling of antennas to reaction centers*, in *Anoxygenic Photosynthetic Bacteria*, R.E. Blankenship, M.T. Madigan, and C.E. Bauer, Editors. 1995, Kluwer Academic Publishers: Dordrecht, The Netherlands. p. 385–398.
38. Cogdell, R.J., et al., *The purple bacterial photosynthetic unit*. *Photosynth. Res.*, 1996. **48**(1–2): p. 55–63.

39. Emerson, R. and W.A. Arnold, *The photochemical reaction in photosynthesis*. J. Gen. Physiol., 1932. **16**: p. 191–205.
40. Aagaard, J. and W.R. Sistrom, Control of synthesis of reaction center bacteriochlorophyll in photosynthetic bacteria. Photochem. Photobiol., 1972. **15**(2): p. 209–25.
41. Polívka, T. and V. Sundström, Ultrafast Dynamics of Carotenoid Excited States—From Solution to Natural and Artificial Systems. Chemical Reviews, 2004. **104**(4): p. 2021–2072.
42. Cogdell, R.J., *Carotenoids in photosynthesis*. Philos. Trans. R. Soc. London, Ser. B, 1978. **284**(1002): p. 569–79.
43. Koepke, J., et al., The crystal structure of the light-harvesting complex II (B800-850) from Rhodospirillum rubrum. Structure, 1996. **4**(5): p. 581–597.
44. McDermott, G., et al., Crystal structure of an integral membrane light-harvesting complex from photosynthetic bacteria. Nature, 1995. **374**(6522): p. 517–521.
45. Papiz, M.Z., et al., The structure and thermal motion of the B800-850 LH2 complex from Rps. acidophila at 2.0 Å resolution at 100 K: New structural features and functionally relevant motions. J. Mol. Biol., 2003. **326**: p. 1523–1538.
46. Walz, T., et al., Projection structures of three photosynthetic complexes from Rhodospirillum rubrum: LH2 at 6 Å, LH1 and RC-LH1 at 25 Å. J. Mol. Biol., 1998. **282**(4): p. 833–845.
47. Freer, A., et al., Pigment-pigment interactions and energy transfer in the antenna complex of the photosynthetic bacterium Rhodospirillum rubrum. Structure (London), 1996. **4**(4): p. 449–462.
48. Lang, H.P. and C.N. Hunter, The relationship between carotenoid biosynthesis and the assembly of the light-harvesting LH2 complex in Rhodospirillum rubrum. Biochem. J., 1994. **298**(1): p. 197–205.
49. Ritz, T., et al., Excitons and excitation transfer in the photosynthetic unit of purple bacteria. J. Lumin., 1998. **76&77**: p. 310–321.
50. Hu, X., et al., *Photosynthetic apparatus of purple bacteria*. Quart. Rev. Biophys., 2002. **35**: p. 1–62.
51. Van Amerongen, H., L. Valkunas, and R. Van Grondelle, *Photosynthetic Excitons*. 2000: p. 590.
52. Cogdell, R.J., A. Gall, and J. Köhler, The architecture and function of the light-harvesting apparatus of purple bacteria: from single molecules to in vivo membranes. Quart. Rev. Biophys., 2006. **39**: p. 227–324.
53. Niwa, S., et al., Structure of the LH1-RC complex from Thermochromatium tepidum at 3.0 Å resolution. Nature, 2014. **508**(7495): p. 228–232.
54. Scheuring, S., et al., Nanodissection and high-resolution imaging of the Rhodospirillum rubrum photosynthetic core complex in native membranes by AFM. Proceedings of the National Academy of Sciences, 2003. **100**(4): p. 1690–1693.
55. Scheuring, S., et al., *Watching the photosynthetic apparatus in native membranes*. Proceedings of the National Academy of Sciences of the United States of America, 2004. **101**(31): p. 11293–11297.
56. Jamieson, S.J., et al., Projection structure of the photosynthetic reaction centre-antenna complex of Rhodospirillum rubrum at 8.5 Å resolution. The EMBO Journal, 2002. **21**(15): p. 3927–3935.
57. Francia, F., et al., The Reaction Center–LH1 Antenna Complex of Rhodospirillum rubrum Contains One PufX Molecule Which Is Involved in Dimerization of This Complex. Biochemistry, 1999. **38**(21): p. 6834–6845.

58. Roszak, A.W., et al., Crystal structure of the RC-LH1 core complex from *Rhodospseudomonas palustris*. *Science*, 2003. **302**: p. 1969–1972.
59. Comayras, F., C. Jungas, and J. Lavergne, Functional Consequences of the Organization of the Photosynthetic Apparatus in *Rhodobacter sphaeroides*: II. A STUDY OF PufX– MEMBRANES. *Journal of Biological Chemistry*, 2005. **280**(12): p. 11214–11223.
60. Barz, W.P., et al., Role of the PufX protein in photosynthetic growth of *Rhodobacter sphaeroides*. 2. PufX is required for efficient ubiquinone/ubiquinol exchange between the reaction center QB site and the cytochrome bc1 complex. *Biochemistry*, 1995. **34**(46): p. 15248–58.
61. Chi, S.C., et al., Assembly of functional photosystem complexes in *Rhodobacter sphaeroides* incorporating carotenoids from the spirilloxanthin pathway. *Biochimica et Biophysica Acta (BBA) - Bioenergetics*, 2015. **1847**(2): p. 189–201.
62. Bullough, P.A., P. Qian, and C.N. Hunter, eds. *Reaction Center-Light-Harvesting Core Complexes of Purple Bacteria*. *The Purple Phototrophic Bacteria*, ed. F.D. C.N. Hunter, M.C. Thurnauer, J.T. Beatty. Vol. 28. 2009, Springer: Dordrecht, The Netherlands. 155–179.
63. Qian, P., P.A. Bullough, and C.N. Hunter, Three-dimensional Reconstruction of a Membrane-bending Complex: The RC-LH1-Pufx core dimer of *Rhodobacter sphaeroides*. *Journal of Biological Chemistry*, 2008. **283**(20): p. 14002-14011.
64. Qian, P., et al., Three-Dimensional Structure of the *Rhodobacter sphaeroides* RC-LH1-PufX Complex: Dimerization and Quinone Channels Promoted by PufX. *Biochemistry*, 2013. **52**(43): p. 7575–7585.
65. Qian, P., C. Neil Hunter, and P.A. Bullough, *The 8.5 Å Projection Structure of the Core RC-LH1-PufX Dimer of Rhodobacter sphaeroides*. *Journal of Molecular Biology*, 2005. **349**(5): p. 948–960.
66. Sturgis, J.N., et al., *Atomic Force Microscopy Studies of Native Photosynthetic Membranes*. *Biochemistry*, 2009. **48**(17): p. 3679–3698.
67. Jungas, C., et al., Supramolecular organization of the photosynthetic apparatus of *Rhodobacter sphaeroides*. *EMBO Journal*, 1999. **18**(3): p. 534–542.
68. Scheuring, S., et al., Structural Role of PufX in the Dimerization of the Photosynthetic Core Complex of *Rhodobacter sphaeroides*. *Journal of Biological Chemistry*, 2004. **279**(5): p. 3620–3626.
69. Siebert, C.A., et al., Molecular architecture of photosynthetic membranes in *Rhodobacter sphaeroides*: the role of PufX. *EMBO J*, 2004. **23**(4): p. 690–700.
70. Jones, M.R., et al., Mutants of *Rhodobacter sphaeroides* lacking one or more pigment-protein complexes and complementation with reaction-center, LH1, and LH2 genes. *Mol. Microbiol.*, 1992. **6**(9): p. 1173–84.
71. Kirmaier, C. and D. Holten, Primary photochemistry of reaction centers from the photosynthetic purple bacteria. *Photosynth. Res.*, 1987. **13**(3): p. 225–60.
72. Woodbury, N.W. and J.P. Allen, The pathway, kinetics and thermodynamics of electron transfer in wild type and mutant reaction centers of purple nonsulfur bacteria, in *Anoxygenic Photosynthetic Bacteria*, R.E. Blankenship, M.T. Madigan, and C.E. Bauer, Editors. 1995, Kluwer Academic Publishers: Dordrecht. p. 527–557.
73. Parson, W.W. *Photosynthetic bacterial reaction centers*. in *Protein Electron Transfer*. 1996. Minerals, Metals & Materials Society, Warrendale, Pa.
74. Clayton, R.K. and R.T. Wang, *Photochemical reaction centers from Rhodospseudomonas sphaeroides*, in *Meths. Enzyme.*, S.P. Colowick and N.O. Kaplan, Editors. 1971, Academic Press: New York and London. p. 696–704.

75. Feher, G., Some chemical and physical properties of a bacterial reaction center particle and its primary photo-chemical reactants. *Photochem. photobiol.*, 1971. **14**: p. 373–387.
76. Allen, J.P., et al., *Structure of the reaction center from Rhodobacter sphaeroides R-26: the cofactors*. *Proc. Natl. Acad. Sci. U. S. A.*, 1987. **84**(16): p. 5730–4.
77. Allen, J.P., et al., *Structure of the reaction center from Rhodobacter sphaeroides R-26: the protein subunits*. *Proceedings of the National Academy of Sciences*, 1987. **84**(17): p. 6162–6166.
78. Chang, C.H., et al., Structure of the membrane-bound protein photosynthetic reaction center from *Rhodobacter sphaeroides*. *Biochemistry*, 1991. **30**(22): p. 5352–5360.
79. Ermler, U., et al., Structure of the photosynthetic reaction centre from *Rhodobacter sphaeroides* at 2.65 Å resolution: cofactors and protein-cofactor interactions. *Structure*, 1994. **2**: p. 925–936.
80. McAuley, K.E., et al., X-ray crystal structure of the YM210W mutant reaction centre from *Rhodobacter sphaeroides*. *FEBS Letters*, 2000. **467**(2–3): p. 285–290.
81. Katona, G., et al., Lipidic Cubic Phase Crystal Structure of the Photosynthetic Reaction Centre from *Rhodobacter sphaeroides* at 2.35 Å Resolution. *Journal of Molecular Biology*, 2003. **331**(3): p. 681–692.
82. Chang, C.H., et al., Structure of *Rhodospseudomonas sphaeroides* R-26 reaction center. *FEBS Lett.*, 1986. **205**(1): p. 82–6.
83. Feher, G., et al., *Structure and function of bacterial photosynthetic reaction centers*. *Nature (London)*, 1989. **339**(6220): p. 111–16.
84. Clayton, R.K. Trapping of energy at photosynthetic reaction centers. in *Curr. Photosynth., Proc. West-Eur. Conf.*, 2nd. 1966.
85. Deisenhofer, J. and H. Michel, *High-resolution structures of photosynthetic reaction centers*. *Annu. Rev. Biophys. Biophys. Chem.*, 1991. **20**: p. 247–66.
86. Breton, J., A. Vermeglio, and Editors., *Photosynthetic Bacterial Reaction Center II: Structure, Spectroscopy, and Dynamics*, *Proceedings of NATO Advanced Workshop held at the Maison d'Hotes of the Centre d'Etudes Nuclearies de Cadarache, Aix-en-Provence, France, May 10–15, 1992*. [In: *NATO ASI Ser., Ser A*, 1992; 237]. 1992: Plenum, New York, N. Y. 429.
87. Deisenhofer, J.N., J. R., ed. *The Photosynthetic Reaction Center*. Vol. I and II. 1993, Academic Press.: San Diego.
88. Fleming, G.R. and R. Van Grondelle, The primary steps of photosynthesis the two important initial steps of photosynthesis—electron transfer and energy transfer—occur with great speed and efficiency. new techniques in laser optics and genetic engineering are helping us to. *Phys. Today*, 1994. **47**(2): p. 48–55.
89. Lancaster, C.R.D., U. Ermler, and H. Michel, The structure of photosynthetic reaction centers from purple bacteria as revealed by X-ray crystallography, in *Anoxygenic photosynthetic bacteria*, R.E. Blankenship, M.T. Madigan, and C.E. Bauer, Editors. 1995, Kluwer academic publishers: Dordrecht. p. 503–526.
90. Woodbury, N.W. and J.P. Allen, The pathway, kinetics and thermodynamics of electron transfer in wild type and mutant reaction centers of purple nonsulfur bacteria. *Adv. Photosynth.*, 1995. **2**(Anoxygenic Photosynthetic Bacteria): p. 527–57.
91. Michel-Beyerle, M.E., *Reaction Centers of Photosynthetic Bacteria. Structure and Dynamics*. 1996, Springer-Verlag: Berlin.
92. Hoff, A.J. and J. Deisenhofer, Photophysics of photosynthesis. Structure and spectroscopy of reaction centers of purple bacteria. *Phys. Rep.*, 1997. **287**(1 & 2): p. 1–247.

93. Pfenning, N. General physiology and ecology of photosynthetic bacteria. in Photosynth. Bact. 1978. Plenum, New York, N.
94. Scheuring, S. and J.N. Sturgis, *Chromatic Adaptation of Photosynthetic Membranes*. Science, 2005. **309**(5733): p. 484–487.
95. Adams, P.G. and C.N. Hunter, *Adaptation of intracytoplasmic membranes to altered light intensity in Rhodobacter sphaeroides*. Biochimica et Biophysica Acta (BBA) – Bioenergetics, 2012. **1817**(9): p. 1616–1627.
96. Evans, M.B., A.M. Hawthornthwaite, and R.J. Cogdell, Isolation and characterization of the different B800-850 light-harvesting complexes from low- and high-light grown cells of Rhodospseudomonas palustris, strain 2.1.6. Biochim. Biophys. Acta, 1990. **1016**(1): p. 71–6.
97. Hartigan, N., et al., The 7.5-Å Electron Density and Spectroscopic Properties of a Novel Low-Light B800 LH2 from Rhodospseudomonas palustris. Biophysical journal, 2002. **82**(2): p. 963–977.
98. McLuskey, K., et al., The crystallographic structure of the B800-820 LH3 light-harvesting complex from the purple bacteria Rhodospseudomonas acidophila stain 7050. Biochemistry, 2001. **40**: p. 8783–8789.
99. Freiberg, A., K. Timpmann, and G. Trinkunas, *Spectral fine-tuning in excitonically coupled cyclic photosynthetic antennas*. Chemical Physics Letters, 2010. **500**(1–3): p. 111–115.
100. Cogdell, R.J., et al., The isolation and partial characterization of the light-harvesting pigment-protein complement of Rhodospseudomonas acidophila. Biochim. Biophys. Acta, 1983. **722**(3): p. 427–435.
101. Gardiner, A.T., R.J. Cogdell, and S. Takaichi, The effect of growth conditions on the light-harvesting apparatus in Rhodospseudomonas acidophila. Photosynth. Res., 1993. **38**(2): p. 159–67.
102. Chenchiliyan, M., et al., *Dimerization of core complexes as an efficient strategy for energy trapping in Rhodobacter sphaeroides*. Biochimica et Biophysica Acta (BBA) – Bioenergetics, 2016. **1857**(6): p. 634–642.
103. Timpmann, K., et al., *Efficiency of light harvesting in a photosynthetic bacterium adapted to different levels of light*. Biochimica et Biophysica Acta (BBA) – Bioenergetics, 2014. **1837**(10): p. 1835–1846.
104. Cogdell, R.J., et al., Structure, Function and Biogenesis of Chlorophyll-Protein Complexes. [In: Photosynth. Res., 1995; 44(1–2)]. 1995: Kluwer, Dordrecht, Neth. 219.
105. Şener, M., et al., Photosynthetic Vesicle Architecture and Constraints on Efficient Energy Harvesting. Biophysical journal, 2010. **99**(1): p. 67–75.
106. Hu, X. and K. Schulten, Model for the light-harvesting complex I (B875) of Rhodobacter sphaeroides. Biophys. J., 1998. **75**(2): p. 683–694.
107. Mukamel, S., Principles of Nonlinear Optical Spectroscopy. 1995: Oxford, New York.
108. Sundström, V., T. Pullerits, and R. van Grondelle, Photosynthetic light-harvesting: Reconciling dynamics and structure of purple bacterial LH2 reveals function of photosynthetic unit. J. Phys. Chem. B, 1999. **103**(13): p. 2327–2346.
109. Grondelle, R.v., et al., *Energy transfer and trapping in photosynthesis*. Biochim. Biophys. Acta, 1994. **1187**(1): p. 1–65.
110. Scholes, G.D. and G.R. Fleming, On the mechanism of light harvesting in photosynthetic purple bacteria: B800 to B850 energy transfer. J. Phys. Chem. B, 2000. **104**: p. 1854–1868.

111. Sumi, H., Bacterial photosynthesis begins with quantum-mechanical coherence. *The Chemical Record*, 2000. **1**: p. 480–493.
112. Chachisvilis, M., et al., Excitons in photosynthetic purple bacteria: Wavelike motion or incoherent hopping? *J. Phys. Chem. B*, 1997. **101**(37): p. 7275–7283.
113. Dahlbom, M., et al., Exciton delocalization in the B850 light-harvesting complex: Comparison of different measures. *J. Phys. Chem. B*, 2001. **105**(23): p. 5515–5524.
114. Damjanovic, A., et al., Excitons in a photosynthetic light-harvesting system: A combined molecular dynamics, quantum chemistry, and polaron model study. *Phys. Rev. E*, 2002. **65**: p. 031919–031943.
115. Timpmann, K., et al., *Bandwidth of excitons in LH2 bacterial antenna chromoproteins*. *Chem. Phys. Lett.*, 2004. **398**: p. 384–388.
116. Freiberg, A., et al., Excitonic polarons in quasi-one-dimensional LH1 and LH2 bacteriochlorophyll a antenna aggregates from photosynthetic bacteria: A wavelength-dependent selective spectroscopy study. *Chemical Physics*, 2009. **357**(1–3): p. 102–112.
117. Freiberg, A., M. Rätsep, and K. Timpmann, A comparative spectroscopic and kinetic study of photoexcitations in detergent-isolated and membrane-embedded LH2 light-harvesting complexes. *Biochimica et Biophysica Acta (BBA) – Bioenergetics*, 2012. **1817**(8): p. 1471–1482.
118. Davydov, A.S., *Theory of Molecular Excitons*. 1971, New York: Plenum Press.
119. Wu, H.-M., et al., Comparison of the LH2 antenna complexes of *Rhodospseudomonas acidophila* (strain 10050) and *Rhodobacter sphaeroides* by high-pressure absorption, high-pressure hole burning, and temperature-dependent absorption spectroscopies. *J Phys. Chem. B*, 1997. **101**(38): p. 7641–7653.
120. Pajusalu, M., et al., Davydov Splitting of Excitons in Cyclic Bacteriochlorophyll a Nanoaggregates of Bacterial Light-Harvesting Complexes between 4.5 and 263 K. *ChemPhysChem*, 2011. **12**(3): p. 634–644.
121. Linnanto, J., J.E.I. Korppi-Tommola, and V.M. Helenius, Electronic States, Absorption Spectrum and Circular Dichroism Spectrum of the Photosynthetic Bacterial LH2 Antenna of *Rhodospseudomonas acidophila* as Predicted by Exciton Theory and Semiempirical Calculations. *J. Phys. Chem. B*, 1999. **103**: p. 8739–8750.
122. Şener, M., et al., Structural model and excitonic properties of the dimeric RC–LH1–PufX complex from *Rhodobacter sphaeroides*. *Chemical Physics*, 2009. **357**(1–3): p. 188–197.
123. Frenkel, J., *On the Transformation of light into Heat in Solids. I*. *Physical Review*, 1931. **37**(1): p. 17–44.
124. Frenkel, J., *On the Transformation of Light into Heat in Solids. II*. *Physical Review*, 1931. **37**(10): p. 1276–1294.
125. Freiberg, A., M. Pajusalu, and M. Rätsep, *Excitons in Intact Cells of Photosynthetic Bacteria*. *The Journal of Physical Chemistry B*, 2013. **117**(38): p. 11007–11014.
126. Harel, E. and G.S. Engel, *Quantum coherence spectroscopy reveals complex dynamics in bacterial light-harvesting complex 2 (LH2)*. *Proceedings of the National Academy of Sciences*, 2012. **109**(3): p. 706–711.
127. Panitchayangkoon, G., et al., *Direct evidence of quantum transport in photosynthetic light-harvesting complexes*. *Proceedings of the National Academy of Sciences*, 2011. **108**(52): p. 20908–20912.

128. Panitchayangkoon, G., et al., *Long-lived quantum coherence in photosynthetic complexes at physiological temperature*. Proceedings of the National Academy of Sciences, 2010. **107**(29): p. 12766–12770.
129. Förster, T., *Zwischenmolekulare Energiewanderung und Fluoreszenz*. Annalen der Physik, 1948. **437**(1–2): p. 55–75.
130. Sumi, H., Theory of rates of excitation-energy transfer between molecular aggregates through distributed transition dipoles with application to the antenna system in bacterial photosynthesis. *J. Phys. Chem. B*, 1999. **103**: p. 252–260.
131. Scholes, G.D., X.J. Jordanides, and G.R. Fleming, *Adapting the Förster Theory of Energy Transfer for Modeling Dynamics in Aggregated Molecular Assemblies*. The Journal of Physical Chemistry B, 2001. **105**(8): p. 1640–1651.
132. Jang, S., M.D. Newton, and R.J. Silbey, *Multichromophoric Förster Resonance Energy Transfer*. Physical Review Letters, 2004. **92**(21): p. 218301.
133. Jang, S., M.D. Newton, and R.J. Silbey, Multichromophoric Förster resonance energy transfer from B800 to B850 in the light harvesting complex 2: evidence for subtle energetic optimization by purple bacteria. The Journal of Physical Chemistry B, 2007. **111**(24): p. 6807–6814.
134. Chernyak, V. and S. Mukamel, Collective coordinates for nuclear spectral densities in energy transfer and femtosecond spectroscopy of molecular aggregates. The Journal of Chemical Physics, 1996. **105**(11): p. 4565–4583.
135. Zhang, W.M., et al., Exciton-migration and three-pulse femtosecond optical spectroscopies of photosynthetic antenna complexes. The Journal of Chemical Physics, 1998. **108**(18): p. 7763–7774.
136. Van Grondelle, R. and V.I. Novoderezhkin, *Energy transfer in photosynthesis: experimental insights and quantitative models*. Phys. Chem. Chem. Phys., 2006. **8**: p. 793–807.
137. Scholes, G.D., R.D. Harcourt, and G.R. Fleming, *Electronic interactions in photosynthetic light-harvesting complexes: The role of carotenoids*. J. of Phys. Chem. B, 1997. **101**(37): p. 7302–7312.
138. Ma, Y.-Z., R.J. Cogdell, and T. Gillbro, Energy Transfer and Exciton Annihilation in the B800-850 Antenna Complex of the Photosynthetic Purple Bacterium *Rhodospseudomonas acidophila* (Strain 10050). A Femtosecond Transient Absorption Study. *J. Phys. Chem. B*, 1997. **101**(6): p. 1087–1095.
139. Freiberg, A., et al., Picosecond dynamics of directed excitation transfer in spectrally heterogeneous light-harvesting antenna of purple bacteria. *Biochim. Biophys. Acta*, 1989. **973**(1): p. 93–104.
140. Freiberg, A., et al., Directed picosecond excitation transport in purple photosynthetic bacteria. *Chem. Phys.*, 1988. **128**(1): p. 227–235.
141. Timpmann, K., N.W. Woodbury, and A. Freiberg, *Unraveling exciton relaxation and energy transfer in LH2 photosynthetic antennas*. *J. Phys. Chem. B*, 2000. **104**(42): p. 9769–9771.
142. Borisov, A.Y., et al., Kinetics of picosecond bacteriochlorophyll luminescence in vivo as a function of the reaction center state. *Biochim. Biophys. Acta*, 1985. **807**(3): p. 221–229.
143. Jordanides, X.J., et al., Electronic Couplings and Energy Transfer Dynamics in the Oxidized Primary Electron Donor of the Bacterial Reaction Center. The Journal of Physical Chemistry B, 2004. **108**(5): p. 1753–1765.

144. Trissl, H.W., C.J. Law, and R.J. Cogdell, *Uphill energy transfer in LH2-containing purple bacteria at room temperature*. Biochim. Biophys. Acta, 1999. **1412**(2): p. 149–172.
145. Timpmann, K., et al., Detrapping of excitation energy from the reaction center in the photosynthetic purple bacterium *Rhodospirillum rubrum*. Biochim. Biophys. Acta, 1993. **1183**(1): p. 185–193.
146. Timpmann, K., A. Freiberg, and V. Sundström, Energy trapping and detrapping in the photosynthetic bacterium *Rhodospseudomonas viridis*: transfer-to-trap-limited dynamics. Chem. Phys., 1995. **194**(2,3): p. 275–283.
147. Freiberg, A., et al., Energy trapping and detrapping by wild type and mutant reaction centers of purple non-sulfur bacteria. Photosynth. Res., 1996. **48**(1–2): p. 309–319.
148. Somsen, O.J.G., L. Valkunas, and R. van Grondelle, *A perturbed two-level model for exciton trapping in small photosynthetic systems*. Biophys. J., 1996. **70**(2): p. 669–83.
149. Fassioli, F., et al., Energy Transfer in Light-Adapted Photosynthetic Membranes: From Active to Saturated Photosynthesis. Biophysical journal, 2009. **97**(9): p. 2464–2473.
150. Kiley, P.J. and S. Kaplan, Molecular genetics of photosynthetic membrane biosynthesis in *Rhodobacter sphaeroides*. Microbiological Reviews, 1988. **52**(1): p. 50–69.
151. Zeilstra-Ryalls, J., et al., *Control of Photosystem Formation in Rhodobacter sphaeroides*. Journal of Bacteriology, 1998. **180**(11): p. 2801–2809.
152. Olsen, J.D., et al., Modification of a hydrogen bond to a bacteriochlorophyll a molecule in the light-harvesting 1 antenna of *Rhodobacter sphaeroides*. Proc. Natl. Acad. Sci. U. S. A., 1994. **91**(15): p. 7124–8.
153. Tucker, J.D., et al., Membrane invagination in *Rhodobacter sphaeroides* is initiated at curved regions of the cytoplasmic membrane, then forms both budded and fully detached spherical vesicles. Molecular Microbiology, 2010. **76**(4): p. 833–847.
154. Niederman, R.A., D.E. Mallon, and L.C. Parks, Membranes of *Rhodospseudomonas sphaeroides*. VI. Isolation of a fraction enriched in newly synthesized bacteriochlorophyll a-protein complexes. Biochim. Biophys. Acta, 1979. **555**(2): p. 210–220.
155. Ratcliffe, E.C., et al., Experimental evidence that the membrane-spanning helix of PufX adopts a bent conformation that facilitates dimerisation of the *Rhodobacter sphaeroides* RC–LH1 complex through N-terminal interactions. Biochimica et Biophysica Acta (BBA) – Bioenergetics, 2011. **1807**(1): p. 95–107.
156. Adams, P.G., et al., Monomeric RC–LH1 core complexes retard LH2 assembly and intracytoplasmic membrane formation in PufX-minus mutants of *Rhodobacter sphaeroides*. Biochimica et Biophysica Acta (BBA) – Bioenergetics, 2011. **1807**(9): p. 1044–1055.
157. Holden-Dye, K., L.I. Crouch, and M.R. Jones, *Structure, function and interactions of the PufX protein*. Biochimica et Biophysica Acta (BBA) – Bioenergetics, 2008. **1777**(7–8): p. 613–630.
158. Valkunas, L., V. Liuolia, and A. Freiberg, *Picosecond processes in chromatophores at various excitation intensities*. Photosynth. Res., 1991. **27**(2): p. 83–95.
159. Van Grondelle, R., Excitation energy transfer, trapping and annihilation in photosynthetic systems. Biochim. Biophys. Acta, 1985. **811**(2): p. 147–95.

160. Bakker, J.G.C., R. Van Grondelle, and W.T.F. Den Hollander, Trapping, loss and annihilation of excitations in a photosynthetic system. II. Experiments with the purple bacteria *Rhodospirillum rubrum* and *Rhodopseudomonas capsulata*. *Biochim. Biophys. Acta*, 1983. **725**(3): p. 508–18.
161. Paillotin, G., N.E. Geacintov, and J. Breton, A master equation theory of fluorescence induction, photochemical yield, and singlet-triplet exciton quenching in photosynthetic systems. *Biophysical journal*, 1983. **44**(1): p. 65–77.
162. Freiberg, A. and P. Saari, *Picosecond spectrochronography*. *IEEE J. Quantum Electron.*, 1983. **QE-19**(4): p. 622–30.
163. van Resandt, R.W.W., R.H. Vogel, and S.W. Provencher, *Double beam fluorescence lifetime spectrometer with subnanosecond resolution: Application to aqueous tryptophan*. *Review of Scientific Instruments*, 1982. **53**(9): p. 1392–1397.
164. Kinoshita, S., H. Ohta, and T. Kushida, Subnanosecond fluorescence-lifetime measuring system using single photon counting method with mode-locked laser excitation. *Review of Scientific Instruments*, 1981. **52**(4): p. 572–575.
165. Fetisova, Z., et al., Antenna size dependent exciton dynamics in the chlorosomal antenna of the green bacterium *Chloroflexus aurantiacus*. *FEBS Lett.*, 1996. **383**(3): p. 233–6.
166. Comayras, F., C. Jungas, and J. Lavergne, Functional Consequences of the Organization of the Photosynthetic Apparatus in *Rhodobacter sphaeroides*: I. Quinone domains and excitation transfer in chromatophores and reaction center center-antenna complexes. *Journal of Biological Chemistry*, 2005. **280**(12): p. 11203–11213.
167. Freiberg, A., et al., Self-trapped excitons in LH2 antenna complexes between 5 K and ambient temperature. *J. Phys. Chem. B*, 2003. **107**: p. 11510–11519.
168. Timpmann, K., et al., Emitting excitonic polaron states in core LH1 and peripheral LH2 bacterial light-harvesting complexes. *J. Phys. Chem. B*, 2004. **108**: p. 10581–10588.
169. Freiberg, A., et al., *Dual fluorescence of single LH2 antenna nanorings*. *J. Luminescence*, 2004. **108**: p. 107–110.
170. Strümpfer, J. and K. Schulten, Excited state dynamics in photosynthetic reaction center and light harvesting complex I. *J. Chem. Phys.*, 2012. **137**: p. 065101.
171. Pullerits, T. and A. Freiberg, Picosecond fluorescence of simple photosynthetic membranes: evidence of spectral inhomogeneity and directed energy transfer. *Chem. Phys.*, 1991. **149**(3): p. 409–418.
172. Pullerits, T. and A. Freiberg, Kinetic model of primary energy transfer and trapping in photosynthetic membranes. *Biophys. J.*, 1992. **63**(4): p. 879–96.
173. Pullerits, T., et al., Energy transfer in the inhomogeneously broadened core antenna of purple bacteria: a simultaneous fit of low-intensity picosecond absorption and fluorescence kinetics. *Biophys. J.*, 1994. **66**(1): p. 236–248.

CURRICULUM VITAE

Name: Manoop Chenchiliyan
Date of Birth: November 06, 1986, Calicut, India.
Citizenship: Indian
Address: Valachettiyl House
Chemrakkattur Post office, Areacode Via.
Malappuram, Kerala, India-673639.
Telephone: +919847782159
E-mail: cmanoopckr@gmail.com

Education:

2004–2007 B.Sc. in Physics (first class), university of Calicut, Calicut, India.
2008–2011 M.Sc. Tech. in Photonics (first class), National institute of Technology Calicut, Calicut, India.

Professional carrier:

07. – 12. 2011 Lecturer, Department of Physics, National institute of Technology Calicut, Calicut, India.
01. 2016 – Laboratory specialist, Laboratory of Biophysics, Institute of Physics, University of Tartu, Tartu, Estonia.

Scholarships and Awards

2012–2016 European Social Fund's Doctoral Studies and Internationalization Program, DoRa-4, Archimedes Foundation, Estonia.
2014 Kristjan Jaak short-term visits, Archimedes Foundation, Estonia.
2014 DoRa T8 Young Researchers Foreign Trips Grant, Archimedes Foundation, Estonia.
2011–2015 National Overseas Scholarship by the Govt. of India.
2011–2012 Rajiv Gandhi National Fellowship by University Grants Commission, Govt. of India.

List of publication:

1. Timpmann, Kõu; **Chenchiliyan, Manoop**; Jalviste, Erko; Timney, John A; Hunter, C. Neil; Freiberg, Arvi (2014). Efficiency of light harvesting in a photosynthetic bacterium adapted to different levels of light. *Biochimica et Biophysica Acta-Bioenergetics*, 1837(10), 1835–1846.
2. **Chenchiliyan, Manoop**; Timpmann, Kõu; Jalviste, Erko; Adam, G. Peter; Hunter, C. Neil; Freiberg, Arvi (2016). Dimerization of core complexes as an efficient strategy for energy trapping in *Rhodobacter sphaeroides*. *Biochimica et Biophysica Acta-Bioenergetics*, 1857 (6), 634–642.

3. Freiberg, Arvi ; **Chenchiliyan, Manoop**; Rätsep, Margus; Timpmann, Kõu (2016). Spectral and kinetic effects accompanying the assembly of core complexes of *Rhodobacter sphaeroides*. *Biochimica et Biophysica Acta-Bioenergetics*, 1857 (11), 1727–1733.
4. **Chenchiliyan, Manoop**; Palengara, Sudheesh; Varghese, Soney (2011). Transparent electrode patterning using laser ablation for in-plane switching liquid crystal display. *American Institute of Physics conf.proc.1391*, 294–296.

ELULOOKIRJELDUS

Nimi: Manoop Chenchiliyan
Sünniaeg: 06. 11. 1986, Calicut, India
Kodakondsus: India
Kontakt: Valachettiyil House
Chemrakkattur Post office, Areacode Via.
Malappuram, Kerala, India-673639.
Telefon: +919847782159
E-post: cmanoopckr@gmail.com

Haridus:

2004–2007 B.Sc. füüsikas (I klass), Calicut Ülikool, India.
2008–2011 M.Sc. Tech. fotoonikas (I klass), Calicuti Rahvuslik Tehnoloogia Instituut, India.

Professional carrier:

07. – 12. 2011 Calicuti Rahvuslik Tehnoloogia Instituudi Füüsika osakond, lektor (India).
01. 2016 – Tartu Ülikooli Füüsika Instituudi Biofüüsika labor, spetsialist biofüüsika valdkonnas, (Eesti).

Preemiad ja stipendiumid:

2012–2016 Euroopa sotsiaal fondi programm: Doktori õpe ja rahvusvahelistumine, DoRa-4, SA Archimedes, Eesti.
2014 Kristjan Jaagu välissõidu stipendium, SA Archimedes, Estonia.
2014 DoRa T8, Noore Teadlase Välissõitude Toetus (Grant), SA Archimedes, Eesti.
2011–2015 India Valitsuse stipendium doktori õppinguteks väljasvool India Vabariiki.
2011–2012 India Ülikoolide Toetuste Komitee poolt väljastatud Rajiv Gandhi nimeline rahvuslik toetus.

Publikatsioonid:

1. Timpmann, Kõu; **Chenchiliyan, Manoop**; Jalviste, Erko; Timney, John A; Hunter, C. Neil; Freiberg, Arvi (2014). Efficiency of light harvesting in a photosynthetic bacterium adapted to different levels of light. *Biochimica et Biophysica Acta-Bioenergetics*, 1837(10), 1835–1846.
2. **Chenchiliyan, Manoop**; Timpmann, Kõu; Jalviste, Erko; Adam, G. Peter; Hunter, C. Neil; Freiberg, Arvi (2016). Dimerization of core complexes as an efficient strategy for energy trapping in *Rhodobacter sphaeroides*. *Biochimica et Biophysica Acta-Bioenergetics*, 1857 (6), 634–642.

3. Freiberg, Arvi ; **Chenchiliyan, Manoop**; Rätsep, Margus; Timpmann, Kõu (2016). Spectral and kinetic effects accompanying the assembly of core complexes of *Rhodobacter sphaeroides*. *Biochimica et Biophysica Acta-Bioenergetics*, 1857 (11), 1727–1733.
4. **Chenchiliyan, Manoop**; Palengara, Sudheesh; Varghese, Soney (2011). Transparent electrode patterning using laser ablation for in-plane switching liquid crystal display. *American Institute of Physics conf.proc.1391*, 294-296.

DISSERTATIONES PHYSICAE UNIVERSITATIS TARTUENSIS

1. **Andrus Ausmees.** XUV-induced electron emission and electron-phonon interaction in alkali halides. Tartu, 1991.
2. **Heiki Sõnajalg.** Shaping and recalling of light pulses by optical elements based on spectral hole burning. Tartu, 1991.
3. **Sergei Savihhin.** Ultrafast dynamics of F-centers and bound excitons from picosecond spectroscopy data. Tartu, 1991.
4. **Ergo Nõmmiste.** Leelishalogeniidide röntgenelektronemissioon kiiritamisel footonitega energiaga 70–140 eV. Tartu, 1991.
5. **Margus Rätsep.** Spectral gratings and their relaxation in some low-temperature impurity-doped glasses and crystals. Tartu, 1991.
6. **Tõnu Pullerits.** Primary energy transfer in photosynthesis. Model calculations. Tartu, 1991.
7. **Olev Saks.** Attoampri diapsoonis voolude mõõtmise füüsikalised alused. Tartu, 1991.
8. **Andres Virro.** AlGaAsSb/GaSb heterostructure injection lasers. Tartu, 1991.
9. **Hans Korge.** Investigation of negative point discharge in pure nitrogen at atmospheric pressure. Tartu, 1992.
10. **Jüri Maksimov.** Nonlinear generation of laser VUV radiation for high-resolution spectroscopy. Tartu, 1992.
11. **Mark Aizengendler.** Photostimulated transformation of aggregate defects and spectral hole burning in a neutron-irradiated sapphire. Tartu, 1992.
12. **Hele Siimon.** Atomic layer molecular beam epitaxy of A^2B^6 compounds described on the basis of kinetic equations model. Tartu, 1992.
13. **Tõnu Reinot.** The kinetics of polariton luminescence, energy transfer and relaxation in anthracene. Tartu, 1992.
14. **Toomas Rõõm.** Paramagnetic H^{2-} and F^+ centers in CaO crystals: spectra, relaxation and recombination luminescence. Tallinn, 1993.
15. **Erko Jalviste.** Laser spectroscopy of some jet-cooled organic molecules. Tartu, 1993.
16. **Alvo Aabloo.** Studies of crystalline celluloses using potential energy calculations. Tartu, 1994.
17. **Peeter Paris.** Initiation of corona pulses. Tartu, 1994.
18. **Павел Рубин.** Локальные дефектные состояния в CuO_2 плоскостях высокотемпературных сверхпроводников. Тарту, 1994.
19. **Olavi Ollikainen.** Applications of persistent spectral hole burning in ultrafast optical neural networks, time-resolved spectroscopy and holographic interferometry. Tartu, 1996.
20. **Ülo Mets.** Methodological aspects of fluorescence correlation spectroscopy. Tartu, 1996.
21. **Mikhail Danilkin.** Interaction of intrinsic and impurity defects in CaS:Eu luminophors. Tartu, 1997.

22. **Ирина Кудрявцева.** Создание и стабилизация дефектов в кристаллах KBr, KCl, RbCl при облучении ВУФ-радиацией. Тарту, 1997.
23. **Andres Osvet.** Photochromic properties of radiation-induced defects in diamond. Tartu, 1998.
24. **Jüri Örd.** Classical and quantum aspects of geodesic multiplication. Tartu, 1998.
25. **Priit Sarv.** High resolution solid-state NMR studies of zeolites. Tartu, 1998.
26. **Сергей Долгов.** Электронные возбуждения и дефектообразование в некоторых оксидах металлов. Тарту, 1998.
27. **Kaupo Kukli.** Atomic layer deposition of artificially structured dielectric materials. Tartu, 1999.
28. **Ivo Heinmaa.** Nuclear resonance studies of local structure in $\text{RBa}_2\text{Cu}_3\text{O}_{6+x}$ compounds. Tartu, 1999.
29. **Aleksander Shelkan.** Hole states in CuO_2 planes of high temperature superconducting materials. Tartu, 1999.
30. **Dmitri Nevedrov.** Nonlinear effects in quantum lattices. Tartu, 1999.
31. **Rein Ruus.** Collapse of 3d (4f) orbitals in 2p (3d) excited configurations and its effect on the x-ray and electron spectra. Tartu, 1999.
32. **Valter Zazubovich.** Local relaxation in incommensurate and glassy solids studied by Spectral Hole Burning. Tartu, 1999.
33. **Indrek Reimand.** Picosecond dynamics of optical excitations in GaAs and other excitonic systems. Tartu, 2000.
34. **Vladimir Babin.** Spectroscopy of exciton states in some halide macro- and nanocrystals. Tartu, 2001.
35. **Toomas Plank.** Positive corona at combined DC and AC voltage. Tartu, 2001.
36. **Kristjan Leiger.** Pressure-induced effects in inhomogeneous spectra of doped solids. Tartu, 2002.
37. **Helle Kaasik.** Nonperturbative theory of multiphonon vibrational relaxation and nonradiative transitions. Tartu, 2002.
38. **Tõnu Laas.** Propagation of waves in curved spacetimes. Tartu, 2002.
39. **Rünno Lõhmus.** Application of novel hybrid methods in SPM studies of nanostructural materials. Tartu, 2002.
40. **Kaido Reivelt.** Optical implementation of propagation-invariant pulsed free-space wave fields. Tartu, 2003.
41. **Heiki Kasemägi.** The effect of nanoparticle additives on lithium-ion mobility in a polymer electrolyte. Tartu, 2003.
42. **Villu Repän.** Low current mode of negative corona. Tartu, 2004.
43. **Алексей Котлов.** Оксиданионные диэлектрические кристаллы: зонная структура и электронные возбуждения. Тарту, 2004.
44. **Jaak Talts.** Continuous non-invasive blood pressure measurement: comparative and methodological studies of the differential servo-oscillometric method. Tartu, 2004.
45. **Margus Saal.** Studies of pre-big bang and braneworld cosmology. Tartu, 2004.

46. **Eduard Gerškevitš.** Dose to bone marrow and leukaemia risk in external beam radiotherapy of prostate cancer. Tartu, 2005.
47. **Sergey Shchemelyov.** Sum-frequency generation and multiphoton ionization in xenon under excitation by conical laser beams. Tartu, 2006.
48. **Valter Kiisk.** Optical investigation of metal-oxide thin films. Tartu, 2006.
49. **Jaan Aarik.** Atomic layer deposition of titanium, zirconium and hafnium dioxides: growth mechanisms and properties of thin films. Tartu, 2007.
50. **Astrid Rekker.** Colored-noise-controlled anomalous transport and phase transitions in complex systems. Tartu, 2007.
51. **Andres Punning.** Electromechanical characterization of ionic polymer-metal composite sensing actuators. Tartu, 2007.
52. **Indrek Jõgi.** Conduction mechanisms in thin atomic layer deposited films containing TiO₂. Tartu, 2007.
53. **Aleksei Krasnikov.** Luminescence and defects creation processes in lead tungstate crystals. Tartu, 2007.
54. **Küllike Rägo.** Superconducting properties of MgB₂ in a scenario with intra- and interband pairing channels. Tartu, 2008.
55. **Els Heinsalu.** Normal and anomalously slow diffusion under external fields. Tartu, 2008.
56. **Kuno Kooser.** Soft x-ray induced radiative and nonradiative core-hole decay processes in thin films and solids. Tartu, 2008.
57. **Vadim Boltrushko.** Theory of vibronic transitions with strong nonlinear vibronic interaction in solids. Tartu, 2008.
58. **Andi Hektor.** Neutrino Physics beyond the Standard Model. Tartu, 2008.
59. **Raavo Josepson.** Photoinduced field-assisted electron emission into gases. Tartu, 2008.
60. **Martti Pärs.** Study of spontaneous and photoinduced processes in molecular solids using high-resolution optical spectroscopy. Tartu, 2008.
61. **Kristjan Kannike.** Implications of neutrino masses. Tartu, 2008.
62. **Vigen Issahhanjan.** Hole and interstitial centres in radiation-resistant MgO single crystals. Tartu, 2008.
63. **Veera Krasnenko.** Computational modeling of fluorescent proteins. Tartu, 2008.
64. **Mait Müntel.** Detection of doubly charged higgs boson in the CMS detector. Tartu, 2008.
65. **Kalle Kepler.** Optimisation of patient doses and image quality in diagnostic radiology. Tartu, 2009.
66. **Jüri Raud.** Study of negative glow and positive column regions of capillary HF discharge. Tartu, 2009.
67. **Sven Lange.** Spectroscopic and phase-stabilisation properties of pure and rare-earth ions activated ZrO₂ and HfO₂. Tartu, 2010.
68. **Aarne Kasikov.** Optical characterization of inhomogeneous thin films. Tartu, 2010.
69. **Heli Valtna-Lukner.** Superluminally propagating localized optical pulses. Tartu, 2010.

70. **Artjom Vargunin.** Stochastic and deterministic features of ordering in the systems with a phase transition. Tartu, 2010.
71. **Hannes Liivat.** Probing new physics in e^+e^- annihilations into heavy particles via spin orientation effects. Tartu, 2010.
72. **Tanel Mullari.** On the second order relativistic deviation equation and its applications. Tartu, 2010.
73. **Aleksandr Lissovski.** Pulsed high-pressure discharge in argon: spectroscopic diagnostics, modeling and development. Tartu, 2010.
74. **Aile Tamm.** Atomic layer deposition of high-permittivity insulators from cyclopentadienyl-based precursors. Tartu, 2010.
75. **Janek Uin.** Electrical separation for generating standard aerosols in a wide particle size range. Tartu, 2011.
76. **Svetlana Ganina.** Hajusandmetega ülesanded kui üks võimalus füüsika-õppe efektiivsuse tõstmiseks. Tartu, 2011
77. **Joel Kuusk.** Measurement of top-of-canopy spectral reflectance of forests for developing vegetation radiative transfer models. Tartu, 2011.
78. **Raul Rammula.** Atomic layer deposition of HfO_2 – nucleation, growth and structure development of thin films. Tartu, 2011.
79. **Сергей Наконечный.** Исследование электронно-дырочных и интерстициал-вакансионных процессов в монокристаллах MgO и LiF методами термоактивационной спектроскопии. Тарту, 2011.
80. **Niina Voropajeva.** Elementary excitations near the boundary of a strongly correlated crystal. Tartu, 2011.
81. **Martin Timusk.** Development and characterization of hybrid electro-optical materials. Tartu, 2012, 106 p.
82. **Merle Lust.** Assessment of dose components to Estonian population. Tartu, 2012, 84 p.
83. **Karl Kruusamäe.** Deformation-dependent electrode impedance of ionic electromechanically active polymers. Tartu, 2012, 128 p.
84. **Liis Rebane.** Measurement of the $W \rightarrow \tau\nu$ cross section and a search for a doubly charged Higgs boson decaying to τ -leptons with the CMS detector. Tartu, 2012, 156 p.
85. **Jevgeni Šablonin.** Processes of structural defect creation in pure and doped MgO and NaCl single crystals under condition of low or super high density of electronic excitations. Tartu, 2013, 145 p.
86. **Riho Vendt.** Combined method for establishment and dissemination of the international temperature scale. Tartu, 2013, 108 p.
87. **Peeter Piksarv.** Spatiotemporal characterization of diffractive and non-diffractive light pulses. Tartu, 2013, 156 p.
88. **Anna Šugai.** Creation of structural defects under superhigh-dense irradiation of wide-gap metal oxides. Tartu, 2013, 108 p.
89. **Ivar Kuusik.** Soft X-ray spectroscopy of insulators. Tartu, 2013, 113 p.
90. **Viktor Vabson.** Measurement uncertainty in Estonian Standard Laboratory for Mass. Tartu, 2013, 134 p.

91. **Kaupo Voormansik.** X-band synthetic aperture radar applications for environmental monitoring. Tartu, 2014, 117 p.
92. **Deivid Pugal.** hp-FEM model of IPMC deformation. Tartu, 2014, 143 p.
93. **Siim Pikker.** Modification in the emission and spectral shape of photo-stable fluorophores by nanometallic structures. Tartu, 2014, 98 p.
94. **Mihkel Pajusalu.** Localized Photosynthetic Excitons. Tartu, 2014, 183 p.
95. **Taavi Vaikjärv.** Consideration of non-adiabaticity of the Pseudo-Jahn-Teller effect: contribution of phonons. Tartu, 2014, 129 p.
96. **Martin Vilbaste.** Uncertainty sources and analysis methods in realizing SI units of air humidity in Estonia. Tartu, 2014, 111 p.
97. **Mihkel Rähn.** Experimental nanophotonics: single-photon sources- and nanofiber-related studies. Tartu, 2015, 107 p.
98. **Raul Laasner.** Excited state dynamics under high excitation densities in tungstates. Tartu, 2015, 125 p.
99. **Andris Slavinskis.** EST Cube-1 attitude determination. Tartu, 2015, 104 p.
100. **Karlis Zalite.** Radar Remote Sensing for Monitoring Forest Floods and Agricultural Grasslands. Tartu, 2016, 124 p.
101. **Kaarel Piip.** Development of LIBS for *in-situ* study of ITER relevant materials. Tartu, 2016, 93 p.
102. **Kadri Isakar.** ²¹⁰Pb in Estonian air: long term study of activity concentrations and origin of radioactive lead. Tartu, 2016, 107 p.
103. **Artur Tamm.** High entropy alloys: study of structural properties and irradiation response. Tartu, 2016, 115 p.
104. **Rasmus Talviste.** Atmospheric-pressure He plasma jet: effect of dielectric tube diameter. Tartu, 2016, 107 p.
105. **Andres Tiko.** Measurement of single top quark properties with the CMS detector. Tartu, 2016, 161 p.
106. **Aire Olesk.** Hemiboreal Forest Mapping with Interferometric Synthetic Aperture Radar. Tartu, 2016, 121 p.
107. **Fred Valk.** Nitrogen emission spectrum as a measure of electric field strength in low-temperature gas discharges. Tartu, 2016, 149 p.